Construction and Building Materials 449 (2024) 138440

Contents lists available at ScienceDirect

Construction and Building Materials

journal homepage: www.elsevier.com/locate/conbuildmat

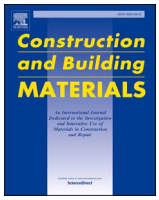

Effects of soil composition and curing conditions on the strength and durability of Cr^{3+}-crosslinked biopolymer-soil composites

Jeong-Uk Bang [a], Minhyeong Lee [b,*], Dong-Yeup Park [a], Ilhan Chang [c], Gye-Chun Cho [a,*]

[a] Department of Civil and Environmental Engineering, Korea Advanced Institute of Science and Technology (KAIST), Daejeon 34141, Republic of Korea
[b] Disposal Safety Evaluation R&D Division, Korea Atomic Energy Research Institute (KAERI), Daedeok-Daero 989-111, Republic of Korea
[c] Department of Civil Systems Engineering, Ajou University, Suwon-si 16499, Republic of Korea

ARTICLE INFO

Keywords:
Biopolymer–soil composite
Soil stabilization
Sand-fine mixture
Fine content
Strength
Durability

ABSTRACT

Stabilized soil composites incorporating Cr^{3+}-crosslinked xanthan gum (CrXG), a self-stiffening cation-crosslinked biopolymer, have recently emerged as sustainable construction materials for earthen structures. However, the influence of curing conditions and soil composition in altering the mechanical properties of CrXG–soil composites has so far received limited attention. This study investigates the effects of fine contents and curing conditions on the time-dependent strength development and durability of CrXG-soil composites. CrXG-soil composites, ranging from poorly graded sand to clayey silty sand, are subjected to unconfined compressive strength (UCS) and durability tests under various curing conditions, including wet, submerged, and dry conditions. Microscopic structural changes are characterized using scanning electron microscopy (SEM) and Fourier-transform infrared spectroscopy (FTIR). The results showed that the UCS of CrXG-soil composite increases nonlinearly, reaching up to 4.8 times the initial wet UCS after 28 days of curing, closely aligning with predictions from a hyperbolic model. Notably, CrXG-soil compositions with a clay-sand mixture (CSM) containing 15 % fine content (CSM_{15}) demonstrated consistent strength parameters across all curing conditions in UCS tests. CSM_{15} also maintains a 90 % of durability index after eight dry-wet cycles and a dry UCS of 300 kPa after 130 days of atmospheric weathering. Microscopic-scale analysis confirms the stable agglomeration of CrXG-clay matrices between sand grains, with the peak wavelength of the major functional group remaining constant, even under multiple cycles. These findings contribute to a deeper understanding of CrXG–soil composites, offering valuable insights into optimizing soil compositions and enhancing the technical feasibility of applying these composites as a sustainable surface protection strategy for earthen structures, such as levees and road slopes.

1. Introduction

Increasing greenhouse gas emissions and extreme weathers resulting from human activities have heightened the frequency and severity of geotechnical engineering hazards, such as landslides [1], levee failures [2], and coastal erosion [3]. Traditionally, cement-based materials [4] accompanied with industrial byproducts, such as fly ash [5] or slag [6], have been the preferred chemical stabilizer for problematic soils, owing to their ease of application, rapid strengthening, and reliable performance [7]. However, cement production contributes approximately 5 % of global CO_2 emissions [8]. Additionally, there are concerns around cement-based soil stabilization, including the elevation of the surrounding soil pH and the release of heavy metals, which can lead to environmental contamination [9]. This can potentially establish a detrimental cycle wherein soil stabilization using cement-based materials inadvertently contributes to greenhouse gas emissions, exacerbating geohazards. Consequently, environmentally friendly biological approaches such as biomineralization and biopolymer treatment have emerged as sustainable alternatives to soil stabilization [10].

Biopolymer-based soil treatment (BPST), which employs biopolymers derived from plants, microorganisms, or fungi, has gained attention for its potential to address challenging ground conditions and mitigate the environmental impact. Notably, biopolymer production emits 4.97 kg of CO_2 per 1 kg [11], significantly lower than the 1.25 tons of CO_2 produced per 1 kg of cement [12]. Polysaccharide biopolymers, such as xanthan gum (XG), guar gum, gellan gum, starch, chitosan, and beta-glucan, have emerged as cost-effective and eco-friendly soil stabilizers. Extensive research has shown that biopolymers can substantially modify the engineering properties of soil through various mechanisms.

* Corresponding authors.
E-mail addresses: leemh@kaeri.re.kr (M. Lee), gyechun@kaist.edu (G.-C. Cho).

https://doi.org/10.1016/j.conbuildmat.2024.138440
Received 21 June 2024; Received in revised form 9 September 2024; Accepted 19 September 2024
Available online 2 October 2024

Nomenclature

BPST	Biopolymer-based soil treatment
CSM	Clay-sand mixture
C_u	Coefficient of uniformity
C_c	Coefficient of curvature
CrXG	Cr^{3+}-crosslinked xanthan gum
DI	Durability index
D_{10}	Effective diameter
ESEM	Environmental scanning electron microscopy
FTIR	Fourier transform infrared spectroscopy
D_{50}	Mean particle size
m_x	Mass of xanthan gum
m_s	Mass of soil
m_w	Mass of water
γ_{dmax}	Maximum dry density
e_{max}	Maximum void ratio
e_{min}	Minimum void ratio
OMC	Optimal water content
k	Rate factor
E_{50}	Secant modulus
U	Strain energy density
SEM	Scanning electron microscopy
G_s	Specific gravity
UCS	Unconfined compressive strength
UCS_{28}	Unconfined compressive strength at 28 days of curing
USCS	Unified soil classification system
XG	Xanthan gum biopolymer
XRD	X-ray diffraction

Their swellable nature increases the viscosity of pore fluids, enhancing both soil binding capabilities and pore infiltration resistance. Upon dehydration, the viscous biopolymer hydrogel condenses into a film with tensile strength, which increases soil cohesion by bringing sand grains closer together, coating their surfaces, and forming mechanical bridges that prevent deformation and detachment [13]. Furthermore, biopolymers interact electrostatically with charged cohesive soils through chemical bonds, such as hydrogen bonds, ionic bonds, and van der Waals forces [14]. These interactions raise the liquid limit and undrained shear strength [15] while promoting clay particle aggregation, thereby facilitating sedimentation [16].

The strength improvement efficiency of biopolymer-treated soil is influenced by several factors, including the biopolymer content relative to the soil mass [17], curing conditions [18], soil type [19], and moisture state [20]. Among these, the biopolymer content plays a crucial role in enhancing strength, with a general trend of increasing strength as biopolymer content rises. However, beyond a certain threshold, the benefits of increased biopolymer content diminish. Choi et al. [17] established that the unconfined compressive strength (UCS) tends to plateau when the biopolymer content exceeds 3 % of the soil mass. Similarly, Hamza et al. [21] observed no significant strength gain in natural soil beyond a 1.5 % biopolymer content. This is consistent with Seo et al. [22], who recommended that the biopolymer content should not exceed 1.5 % for wet-spraying applications in the field, as higher biopolymer contents can hinder uniform mixing due to the increased viscosity of the hydrogel.

XG, an anionic polysaccharide from *Xanthomonas campestris*, has demonstrated significant potential in enhancing soil engineering properties, even at a small dosage (i.e., a mass ratio of XG to soil content (m_x/m_s) of 0.5 %–1 %). For example, Chang et al. [23] reported that a 1 % XG treatment increased the dry UCS of sand to 1.2 MPa and up to 5.5 MPa when fine-grained soils were included. Additionally, Bouazza et al. [24] and Cabalar et al. [25] showed that a 1 % XG treatment reduced the hydraulic conductivity of sand by 3–4 orders of magnitude compared to untreated sand. XG treatment also improves resistance to hydraulic and wind erosion by increasing fluid viscosity and pore filling, as evidenced by a nine-fold increase in the critical shear stress [26] and a significant reduction in weight loss in mine tailings subjected to wind erosion tests [26]. Furthermore, XG-treated soils exhibit enhanced water retention, making them potentially effective in anti-desertification efforts, as shown in studies on residual silt [27] and sand-clay mixtures [28].

These benefits have led to the evaluation of XG-treated soils in various large-scale experiments for reinforcing earthen structures. Seo et al. [22] demonstrated the feasibility of in-situ mixing and pressurized spraying of XG-treated soils on slopes, identifying optimal implementation conditions. Kang et al. [29] found that incorporating 1 % XG-treated soil significantly reduced hydraulic erosion and structural failure in levees during large-scale overtopping experiments. Similarly, Lee et al. [30] reported an increased surface hardness one year after a pilot-scale application of pressurized spraying with XG-treated soil under a bridge abutment. Kwon et al. [31] assessed the effectiveness of a 1 % XG treatment in mitigating internal erosion in earthen embankments through field-scale experiments. However, most studies have focused on short-term performance improvements, leaving the long-term impacts of biopolymer degradation on performance stability relatively unexplored.

Despite the demonstrated improvements in soil properties, significant challenges remain in making XG-stabilized soils viable for field applications. Non-gelling viscous XG hydrogels require dehydration to effectively enhance the compressive strength. Furthermore, even when dehydration-induced strengthening occurs, the effects diminishes if the XG-treated soil reabsorbs water [32]. These limitations complicate the use of XG in environments where dehydration is impractical or where there is constant water exposure in the construction site.

To address these challenges, a cation-crosslinking approach has been developed to enhance the rheological gel strength of XG in its initially hydrated state, as well as to improve water resistance and durability in both the XG hydrogel and XG-treated soils. Cation-crosslinking involves linking electrically charged water-soluble polymer chains via bonding with oppositely charged ions. Upon hydration, the anionic hydroxyl (–OH) and carboxyl (–COOH) groups on the trisaccharide side chains of XG facilitate extensive crosslinking with cations [33]. This polymer–cation cross-linking enlarges the molecular size and weight, transitioning the non-gelling viscous gel to a rigid gel, which exhibits increased yield strength and stiffness. Among various metal cations, Cr^{3+} has shown robust and efficient crosslinking, enhancing the rheological strength of XG hydrogels [34]. When the XG hydrogel interacts with Cr^{3+}, the side chains form a rigid gel with enhanced intermolecular connectivity. The difference in the ionic concentration promotes hydrophobic behavior, reduces water interactions, and prevents reactivation under immersion conditions. Lee et al. [35] demonstrated that a Cr^{3+}-crosslinked XG (CrXG) hydrogel rapidly enhanced the wet UCS in cohesionless sand and maintained strength durability against long-term immersion. Moreover, CrXG–soil stabilization enhances the bearing capacity and reduces permeability through agglomeration and pore filling, highlighting its potential as a construction material for hydraulic barriers in earthen structures [36].

However, significant knowledge gaps remain regarding the four crucial factors essential for demonstrating technical feasibility and widening the potential applications of CrXG–soil stabilization. First, the effect of the soil composition on the strengthening behavior of CrXG treatments, particularly for fine-grained soils, is poorly understood. Many field sites feature weathered soil mixtures composed of sandy and clayey soils, where charged clay particles can affect the interaction with

both biopolymers and cations, which is closely related to the strengthening effect of biopolymer hydrogels in soil. Second, there is limited understanding of the 7-, 14-, and 28-day strengths of CrXG-treated soils, which are typically used design parameters for the construction of geotechnical engineering structures. Third, the strengthening behavior under various curing conditions has not been studied, even though the construction site may experience dry, wet, or saturated conditions, depending on weather events, groundwater level changes, and the surrounding environment. Finally, there is a lack of understanding of the strength durability of CrXG-soil composites although strength durability is an important factor for ensuring performance in field applications. Previous studies have focused exclusively on the strength and durability of poorly graded sands treated with CrXG [35]. Depending on the soil composition and curing conditions, strength durability properties can vary when exposed to cyclic wet-dry conditions. In addition, the strength durability should be evaluated under actual atmospheric weathering conditions in addition to controlled weathering environments.

Therefore, this study aims to deepen the understanding of CrXG–soil stabilization by:

(1) conducting a comprehensive strength assessment of CrXG-treated soils under various soil compositions and curing conditions;

(2) proposing a strength estimation model for nonlinear time-dependent variations using a hyperbolic function;

(3) assessing strength durability under repetitive and atmospheric weathering conditions.

A series of unconfined compressive tests are performed for CrXG-treated soils, varying the fine fraction, curing time, and curing conditions (wet-, saturated-, and dry-cured), coupled with indoor cyclic drying–wetting (D-W) and outdoor durability tests. Furthermore, this study analyzes the microscopic structures of CrXG-treated soils using both conventional and environmental scanning electron microscopy (SEM and ESEM) and Fourier transform infrared spectroscopy (FTIR) to investige the effect of cyclic wet-dry weathering on CrXG-treated soils.

The strengthening effect of CrXG–soil stabilization under variable soil compositions, curing time, and conditions is explored in this study, alongside the strength durability of CrXG-treated soils exposed to controlled and atmospheric weathering conditions. This study provides two main contributions:

(1) A fundamental and mechanistic understanding of the CrXG-induced soil strengthening effect in a wide range of soils, providing optimal sand-fine compositions for soil strengthening depending on the curing environment.

(2) The potential of CrXG treatment as a novel technique to stabilize soils in the construction of earthen structures, such as embankments, abutment slopes, and non-asphalt road pavements.

2. Materials and methods

2.1. Materials

2.1.1. Jumunjin sand and kaolinite clay

This study focuses on understanding how the mechanical properties of CrXG-soil composites change with various fine content from poorly graded sand to clayey silty sand. Therefore, a binary mixture composed of two representative soils (Jumunjin sand and kaolinite clay) was used.

Jumunjin sand was used as a medium-silica base sand. According to the Unified Soil Classification System (USCS), Jumunjin sand is classified as a poorly graded sand (SP) with a mean particle size (D_{50}) of 507 μm. Fig. 1 shows the particle size distribution of Jumunjin sand obtained using a HELOS QUIXEL laser diffraction particle size analyzer (Sympatec Gmbh, Germany), according to ASTM D4464–15 [37]. Table 1 summarizes the geotechnical properties and chemical constituents of the sample by X-ray diffraction (XRD) analysis using an X'Pert Pro Diffractometer (PANalytical, United Kingdom), which showed the dominant silicon dioxide.

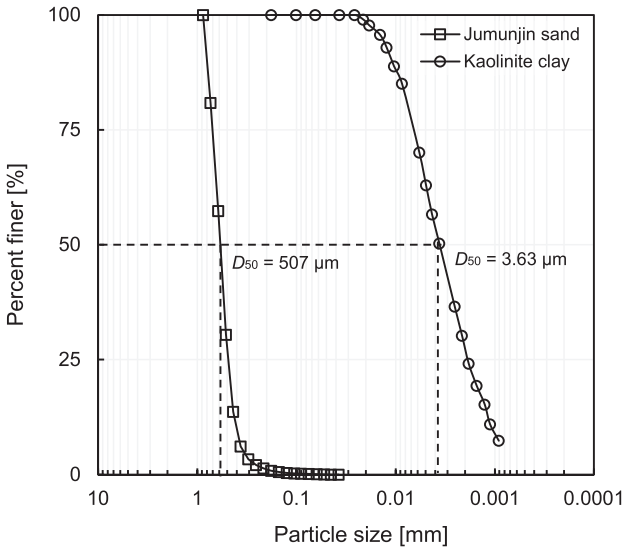

Fig. 1. Particle size distribution curves of Jumunjin sand and kaolinite clay.

Bintang kaolinite clay (Belitung Island, Indonesia) was used as the base fine particles owing to its low cation exchange capacity compared to other clay types. Kaolinite clay is classified as a highly plastic clay (CH) according to the USCS, with plastic and liquid limits of 24 % and 70 %, respectively [38]. The basic soil properties and XRD analysis of kaolinite clay are summarized in Table 1, which indicate that it is the dominant chemical constituent of aluminum silicate. Fig. 1 shows the particle size distribution of kaolinite obtained using the HELOS KR-H2487 laser diffraction particle size analyzer (Sympatec Gmbh, Germany), according to ASTM D4464–15 [37].

2.1.2. Cr^{3+}-crosslinked XG biopolymer

This study utilized research-grade XG powder (CAS No. 11138–66–2; Merck, USA) and chromium nitrate nonahydrate ($Cr(NO_3)_3{\cdot}9\ H_2O$, CAS: 778902–08; Daejung Chemical Co., Korea) to fabricate CrXG gel for soil treatment. $Cr(NO_3)_3{\cdot}9\ H_2O$ was selected as the donor of Cr^{3+} because of its high solubility in Cr^{3+} and stability over a wide pH range [34]. NaCl (CAS: 7647–14–5; Junsei, Korea) was employed as a surface-active agent to reduce repulsive forces and promote binding between XG and Cr^{3+}, facilitating dimeric and polymeric ionic bridging, which was crucial for the gelling mechanism [39]. The presence of NaCl stabilizes the ordered conformation of XG, counteracted electrostatic repulsion between charged groups, and enhanced intermolecular interactions, thereby influencing and controlling the rheology [40].

2.2. Preparation of CrXG-treated soil samples

Fig. 2 outlines the sample preparation and the subsequent experimental investigations. Clay–sand mixtures (CSMs) with varying fine contents were examined to investigate the effects of soil composition on the strengthening behavior of CrXG treatments. Prior to mixing, the Jumunjin sand and kaolinite clay were oven-dried at 110 °C for 24 hours [41] and mixed at clay-to-sand ratios of 0, 5, 10, 15, 20, and 30 % by dry mass. A labeling scheme was applied, following the format CSM_n, where the subscript 'n' denotes the percentage of the clay content. Table 2 summarizes the CSMs used in this study, along with their engineering properties, such as specific gravity (G_s), effective diameter (D_{10}), optimal water content (OMC), and maximum dry density (γ_{dmax}), following ASTM D854–23, D6913, and D698, respectively [42–44].

As the treatment involved mixing CrXG hydrogel with dried CSMs, the initial water content was set above the OMC. Previous studies have shown that a 2 % increase in OMC occurs with a 1 % XG treatment [45], and the OMCs for XG-treated sand-kaolinite mixtures at 75:25 and 50:50

Table 1
Basic soil properties and mineralogical composition of used soil.

Soil	G_s	D_{50} [μm]	C_u	C_c	e_{max}	e_{min}	USCS	Mineralogical composition [%]			
								Quartz	Microcline	Albite	Biotite
Sand	2.65	507	1.94	1.09	0.89	0.64	SP	72	22	6	Trace

Soil	G_s	D_{50} [μm]	LL [%]	PL [%]	PI [%]	SSA [m^2/g]	USCS	Mineralogical composition [%]	
								Kaolinite	Muscovite/Illite
Kaolinite	2.65	3.63	70	24	46	22	CH	89	11

Note: C_u = coefficient of uniformity, C_c= coefficient of curvature, e_{max} = maximum void ratio, e_{min} = minimum void ratio, G_s= specific gravity, PL = plastic limit, LL = liquid limit, PI = plasticity index, and SSA = average specific surface area.

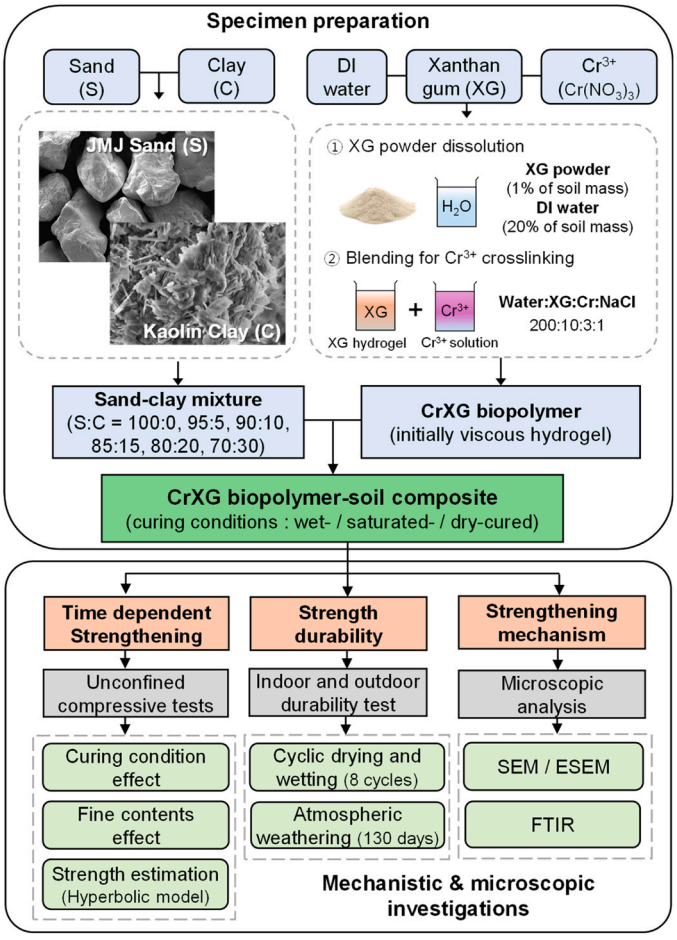

Fig. 2. Summary of the experimental investigations in this study.

Table 2
Compositions of clay-sand mixtures (CSMs).

Label	Composition [%]		G_s [-]	D_{10} [mm]	OMC [%]	γ_{dmax} [kN/m^3]
	Sand	Clay				
CSM_0	100	0	2.623	0.4012	11.1	15.55
CSM_5	95	5	2.618	0.3713	17.0	16.32
CSM_{10}	90	10	2.620	0.2968	18.6	16.73
CSM_{15}	85	15	2.623	0.0081	13.0	17.72
CSM_{20}	80	20	2.626	0.0039	12.6	18.02
CSM_{30}	70	30	2.629	0.0011	14.0	17.93

Note: D_{10} = effective diameter, OMC = optimum moisture content, and γ_{dmax} = maximum dry unit weight.

ratios were reported as 12 % and 20 %, respectively [46]. Low XG dosages can lead to shrinkage cracks due to weak particle bonding [20], while higher XG dosages (>1.5 %) can result in poor workability during wet mixing due to the increased viscosity of the XG hydrogel, particularly in fine-grained soils [47]. Therefore, an XG dosage of 1 % by dry soil mass (m_x/m_s = 1 %) and an initial water content of 20 % were selected to balance soil strengthening efficiency and mixing workability, consistent with previous laboratory [13] and field-scale [22,31] experiments. To prepare the CrXG hydrogel, the optimal crosslinking cation-to-XG mass ratio was determined to be 10:3:1 for XG, Cr $(NO_3)_3{\cdot}9\ H_2O$, and NaCl, as recommended by Lee et al. [35], who evaluated rheological gel strength and treated soil strength under various XG and Cr^{3+} concentrations. Their study found that incorporating Cr(NO3)3·9H2O at 30 % of the XG mass enhanced the gelation rate, leading to more efficient and rapid soil strengthening. However, exceeding this 30 % threshold resulted in syneresis, where water was expelled from the gel matrix, reducing the homogeneity and durability of the treated soil.

The preparation of CrXG-treated soil samples involved three steps. First, a pure XG hydrogel was created by dissolving the XG powder in deionized water at an XG-to-water mass ratio (m_x/m_w) of 5 %, equivalent to m_x/m_s = 1 % at a water content of 20 %. Next, an aqueous Cr^{3+} solution was prepared by dissolving $Cr(NO_3)_3{\cdot}9\ H_2O$ at 30 % of the XG mass along with NaCl at 10 % of the XG mass, using a laboratory stirrer. Equal amounts of pure XG hydrogel and Cr^{3+} solution were combined and mixed at 20,000 rpm for 30 s to obtain a homogenous CrXG gel. The dried CSM with the desired clay–sand ratio was thoroughly mixed with the CrXG gel. The CrXG-treated CSMs were uniformly compacted into a 40 mm cubic mold (Fig. 3) and cured under different conditions, as summarized in Table 3. Due to the extensive range of test conditions, a 40 mm cubical specimen size was chosen for sample preparation and curing. It is important to note that a 40 mm cubic specimen typically shows approximately 15 % higher failure strength compared to the standard cylindrical sample [48].

The curing conditions of the CrXG-treated soil should affect the strengthening characteristics of the CrXG gel because the crosslinking procedure depends on the moisture conditions of the hydrogel [35]. Given the potential for in-situ implementation of CrXG-treated CSMs in various geotechnical applications, this study examined three distinct curing conditions: wet-, saturated-, and dry-cured. The wet-cured conditions, where the samples were kept in a sealed container at room temperature (25 °C) to maintain their initial moisture content (w =

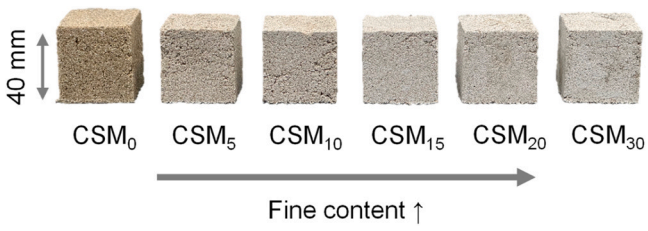

Fig. 3. CrXG biopolymer-soil composite (CSMs) samples.

Table 3
Experimental testing conditions and sample state used in each testing.

Test	Samples	Biopolymer	Curing time	Curing method or, Sample states before testing
Unconfined compressive test	CSM_0, CSM_5, CSM_{10}, CSM_{15}, CSM_{20}, CSM_{30}	CrXG 1 %	0.04, 1, 2, 7, 14, 28 days	-Wet-cured (w = 20 %), -Saturated-cured (w = 24–31 %), -Dry-cured
	CSM_0, CSM_{15}	CrXG 1 %	Wet-cured for 2 days and exposed to cyclic D-W	-Dry or wet state during cycles up to 8
	CSM_0, CSM_{15}	CrXG 1 %	Wet-cured for 2 days and exposed to atmosphere	-In-situ state at 28, 42, 56, 67, 87 and 130 exposure days
SEM	CSM_0, CSM_{15}	CrXG 1 %	Wet-cured for 2 days and exposed to 1 and 8 D-W cycle	-Dry state (RH = 0 %)
ESEM	CSM_0, CSM_{15}	CrXG 1 %	Wet-cured for 2 days and exposed to 1 and 8 D-W cycle	-Wet state (RH = 100 %)
FTIR	CSM_0, CSM_{15}	XG 1 %	Wet-cured for 2 days	-Dry state
		CrXG 1 %	Wet-cured for 2 days and exposed to 4 and 8 D-W cycle	-Dry state

20 %) during curing, simulated subsurface conditions above the groundwater level. In contrast, the saturated-cured condition, where samples were submerged in tap water, represented conditions below the groundwater level. Finally, the dry-cured condition, where samples were cured in an oven at 35 °C, replicated the atmospheric dehydration typically encountered in field environments.

Additionally, this study investigated the impact of the curing duration on strength development by curing CrXG-treated CSMs under the aforementioned conditions for various time periods: 0.04 (~1 hour), 1, 2, 7, 14, and 28 days. The 0.04-day (1 hour) curing condition denotes the interval following sample preparation during which the specimens were demolded and UCS tests were conducted.

2.3. Experiment procedure

2.3.1. UCS test

The UCS values of the CrXG-treated samples were measured using a laboratory universal testing machine (HM-5030.3 F, Humboldt Mfg. Co.). According to ASTM D2166–16, a constant strain rate of 1 %/min (i.e., 0.4 mm/min) was applied until the strain reached 15 % [49]. The UCS values were obtained using the maximum axial stress represented in the stress–strain curves, whereas the secant modulus (E_{50}) was obtained by measuring the slope between the origin and half of the peak strength (1/2 UCS) coordinates for all stress–strain curves. The strain energy density (U), defined as the strain energy per unit volume, represents the amount of energy required to deform soil by breaking inter-particle bonds between soil grains [50]. The strain energy density of CrXG-composites was calculated using the area enclosed by the ascending branch of the stress–strain curve as follows [51]:

$$U = \int_0^{\varepsilon} \sigma \, d\varepsilon \tag{1}$$

where U (kPa) is the strain energy density, σ (kPa) is the stress, and ε is the strain. Three consecutive measurements were averaged for each case to determine three strength parameters.

2.3.2. Durability tests: controlled and atmospheric weathering process

Indoor cyclic D-W and outdoor durability tests were performed using two CrXG-treated soil samples: CSM_0 and CSM_{15} (Fig. 4). The indoor cyclic D-W procedure is illustrated in Fig. 5. Initially, the CrXG-treated soil samples were wet-cured for two days to achieve sufficient initial wet strength. Then, the samples underwent cyclic drying in a 35 °C oven for 48 hours followed by wetting for 24 hours, according to Lee et al. [32] (Fig. 4b). The CrXG-treated soil samples were subjected to eight D-W cycles. UCS tests and density measurements were performed after each D-W procedure.

The strength and water content variations in CrXG-treated soil samples exposed to outdoor atmospheric weathering conditions were also investigated over a 130 day period (from December 2023 to April 2024) at the Korea Advanced Institute of Science and Technology (KAIST, Daejeon, South Korea) (Fig. 4b). A series of cylindrical samples (50 mm in diameter and 100 mm in height) were placed outdoors on a drainable plate to undergo natural D-W cycles. The 130-day duration was selected to ensure the samples experienced sufficient repetitions of D-W cycles, with a particular focus on exposing them to at least 10 instances of precipitation exceeding 10 mm. The sample weights, UCS, and water content were measured after 28, 42, 56, 67, 87, and 130 days of exposure.

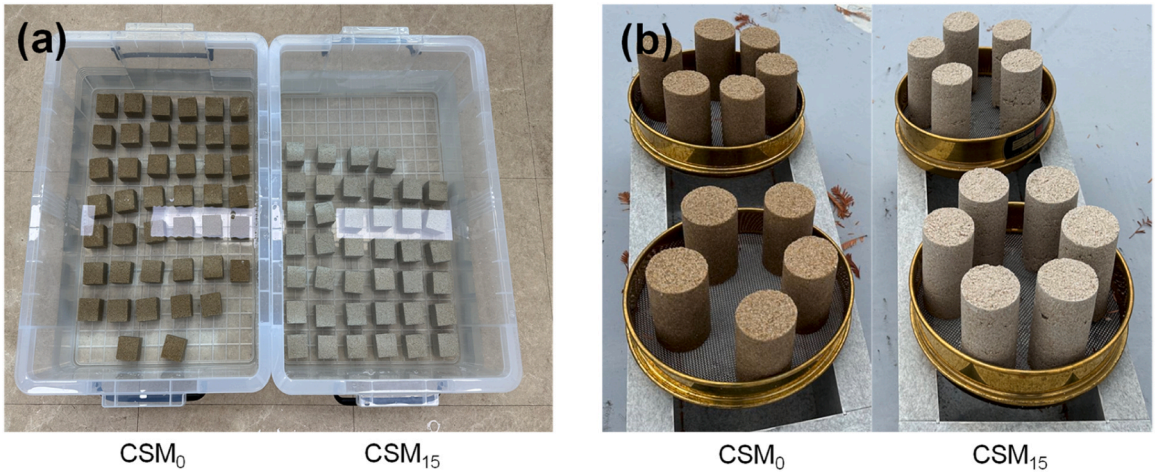

Fig. 4. Indoor and outdoor durability tests. (a) exposure to wetting process, and (b) exposure to atmospheric weathering conditions.

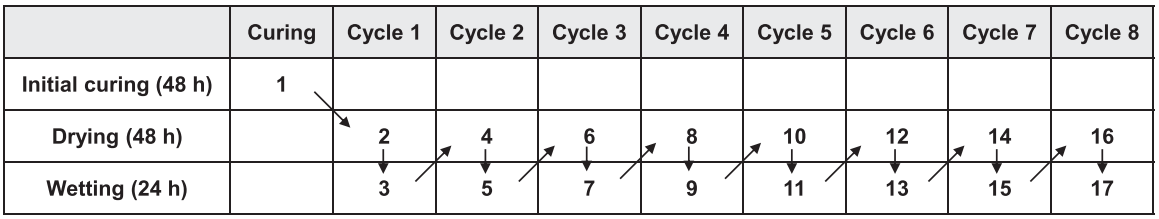

Fig. 5. Cyclic drying-wetting (D-W) procedure.

2.3.3. SEM and ESEM analysis

High-resolution SEM (JSM-IT800, Jeol Ltd.) and ESEM (Quattro ESEM, Thermo Fisher Scientific) observations were performed to investigate the effects of soil composition and D-W weathering on the interaction between the CrXG biopolymer and soil particles. SEM was employed to examine the dry-cured soil samples, which were mounted using a carbon conductive adhesive and coated with platinum to minimize the charging effects. ESEM is a SEM that allows the observation of wet specimens; thus, a humid state was maintained during vacuum processing in the ESEM chamber by regulating the saturated vapor pressure above the freezing point temperature [52], thereby preventing evaporation in wet-cured soil samples.

2.3.4. FTIR analysis

FTIR was used to investigate the changes in the functional groups and chemical bonds resulting from cation-crosslinking between Cr^{3+} and XG as well as the degradation of the CrXG gel after the D-W process. Un-crosslinked XG-, CrXG-, and CrXG-treated samples subjected to four and eight D-W cycles were compared. The samples were placed in a holder cell on an FTIR spectrometer (Nicolet iN10MX, Thermo Fisher Scientific) to obtain a mid-infrared spectrograph (650–4000 cm^{-1}) in accordance with ASTM E1421–99 [53].

3. Results and analysis

3.1. Effect of curing time and curing condition on strength behavior of CrXG-treated soil

Fig. 6 shows the UCS development of the CrXG-treated samples over different curing times (0.04, 1, 2, 7, 14, and 28 days) under three curing conditions: wet, saturated, and dry. Similar to cement-treated soils, which exhibit time-dependent strengthening [5,54], the wet-cured samples exhibited a nonlinear increase in UCS over time, regardless of the fine content (Fig. 6a). CSM_{30} recorded the highest initial UCS value ($UCS_{0.04}$ = 130 kPa), while CSM_0 achieved the highest 28 day strength (UCS_{28} = 363 kPa). Most strengthening occurred within the first day, with the rate of UCS increase gradually decreasing. This is linked to the time-dependent evolution of the yield stress in the XG-Cr^{3+} gel during crosslinking, where the yield stress rapidly increased approximately 21-fold within 24 hours (from 76 to 1610 Pa for the CrXG hydrogel at m_x/m_w = 5 %) before stabilizing [35]. The saturated-cured samples exhibited a similar nonlinear strengthening pattern to wet-cured samples, except for CSM_{30} (Fig. 6b). However, the saturated-cured samples typically displayed lower strength than the wet-cured samples due to the reduced capillary effect which weakened the inter-particle forces [55],

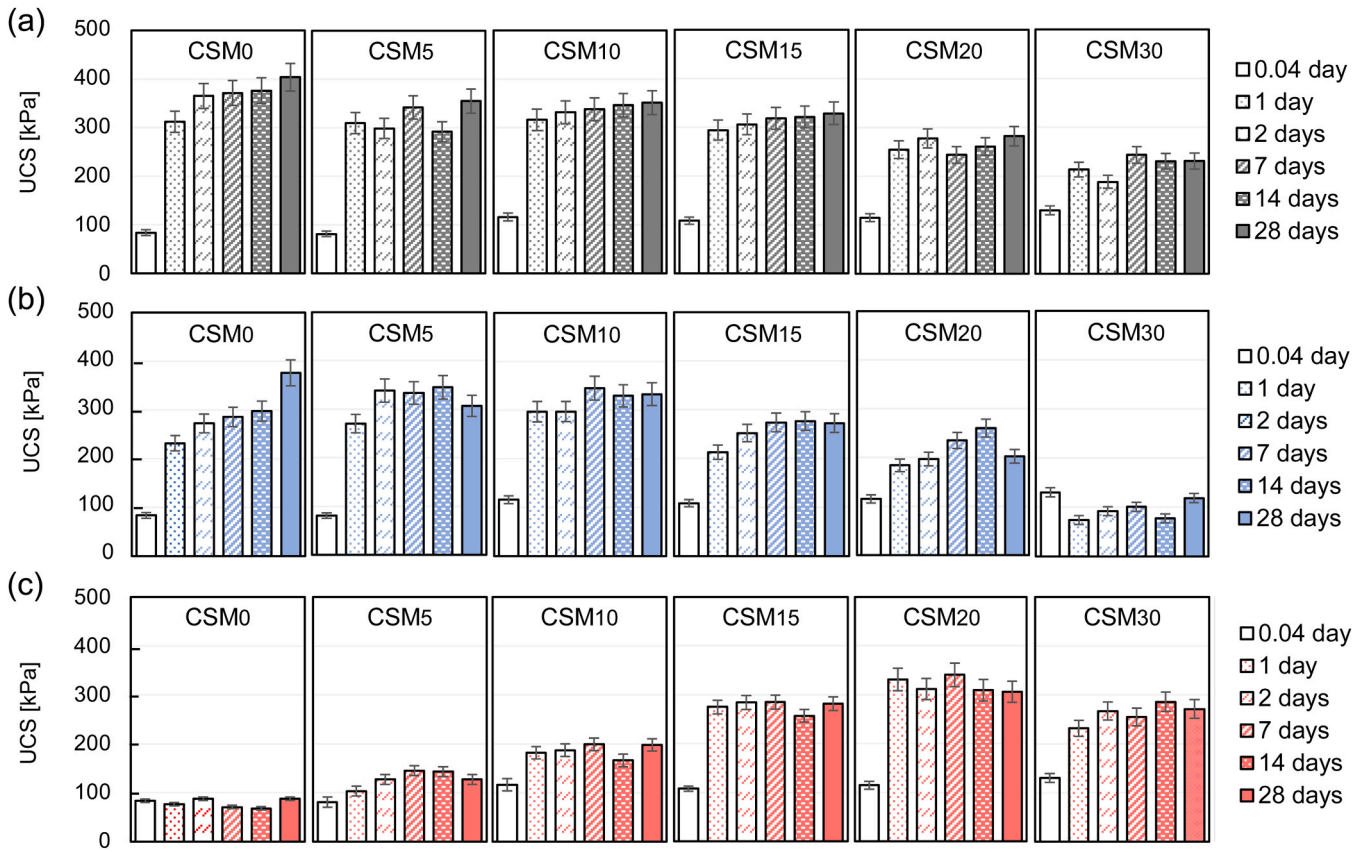

Fig. 6. Time-dependent UCS variations of CrXG biopolymer-soil composite by curing conditions; (a) wet-cured, (b) saturated-cured, and (c) dry-cured.

and the partial softening of the biopolymer gel due to increased water absorption in the saturated condition [56]. Conversely, dry-cured samples exhibited distinctly different strength development (Fig. 6c). UCS values for CSM_0–CSM_{10} were relatively low while CSM_{15}–CSM_{30} showed higher values. Specifically, CSM_0 samples exhibited minimal strength development over the curing period ($UCS_{0.04}$ = 77 kPa and UCS_{28} = 88 kPa). The modest changes in UCS from 1 to 28 days across all dry-cured samples suggest that early dehydration during dry curing impeded time-dependent strengthening in subsequent curing period.

These results illustrate that external conditions substantially influence the nonlinear and time-dependent strength development in CrXG-treated soils, especially for CSM_0 samples, due to variations in the state of the CrXG gel. Under wet- and saturated-cured conditions, the initially viscous CrXG gel transformed into a stiff, hydrated gel, where strength development was driven by the formation of a structural backbone within the XG-Cr^{3+} network, as polymer chains bonded with cations [57]. In contrast, under dry-cured conditions, the CrXG gel transitioned to a thin film due to water evaporation, which caused rapid condensation of XG chains early in the curing process, inhibiting further bonding between polymer chains and cations. This lack of progressive strengthening in dry-cured samples was compounded by volumetric shrinkage in the CrXG film, leading to surface cracking and reduced inter-granular connectivity among sand grains [35]. As a result, dry-cured CSM_0 samples exhibit only a quarter of the UCS observed in wet-cured samples. The inclusion of fines content increased the complexity of these strength-development characteristics, which varied with the curing condition, as further discussed in Section 3.2.

3.2. *Effect of fine content on strength behavior depending on curing environment*

Fig. 7 shows the stress–strain relationships of the CrXG-treated samples cured for 28 days with varying soil compositions. Wet- and saturated-cured samples without fine content (CSM_0) exhibited brittle failure characterized by a high peak stress and low failure strain (< 5 %) (Figs. 7a and 7b), which was mainly derived from the brittle gel fracturing [35]. As the fine content increased in wet- and saturated-cured samples, more ductile failure with a decreased peak stress and increased failure strain (> 10 %) were observed. Fig. 8 shows the UCS_{28}, E_{50}, and U values of the wet-, and saturated-samples with respect to the fine content. The wet- and saturated-cured samples showed a decrease in UCS_{28} and E_{50} with increasing fine content (Figs. 8a and 8b). The UCS_{28} of wet- and saturated-cured samples was reduced by 36 % and 68 % compared to the pure sand condition (CSM_0), respectively, when 30 % fine content was included (Table 4).

From the decreasing trends of UCS and E_{50} with fine content, the influence of fine-grained soil on CrXG-soil composite strength in wet- and saturated-cured conditions can be explained by two mechanisms:

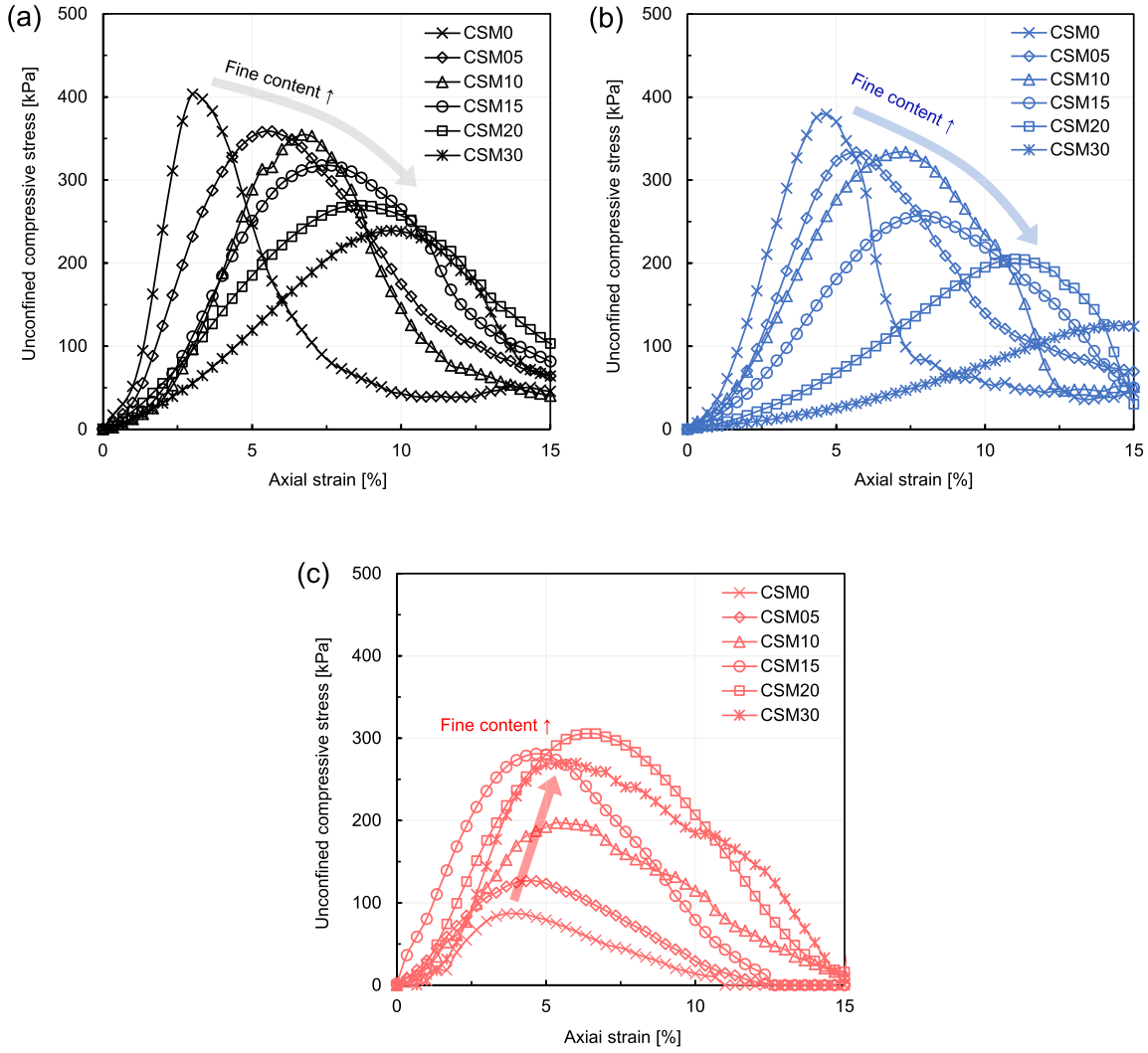

Fig. 7. Stress-strain curve for 28-days-cured CrXG biopolymer-soil composite by fine contents; (a) wet-cured, (b) saturated-cured, and (c) dry-cured.

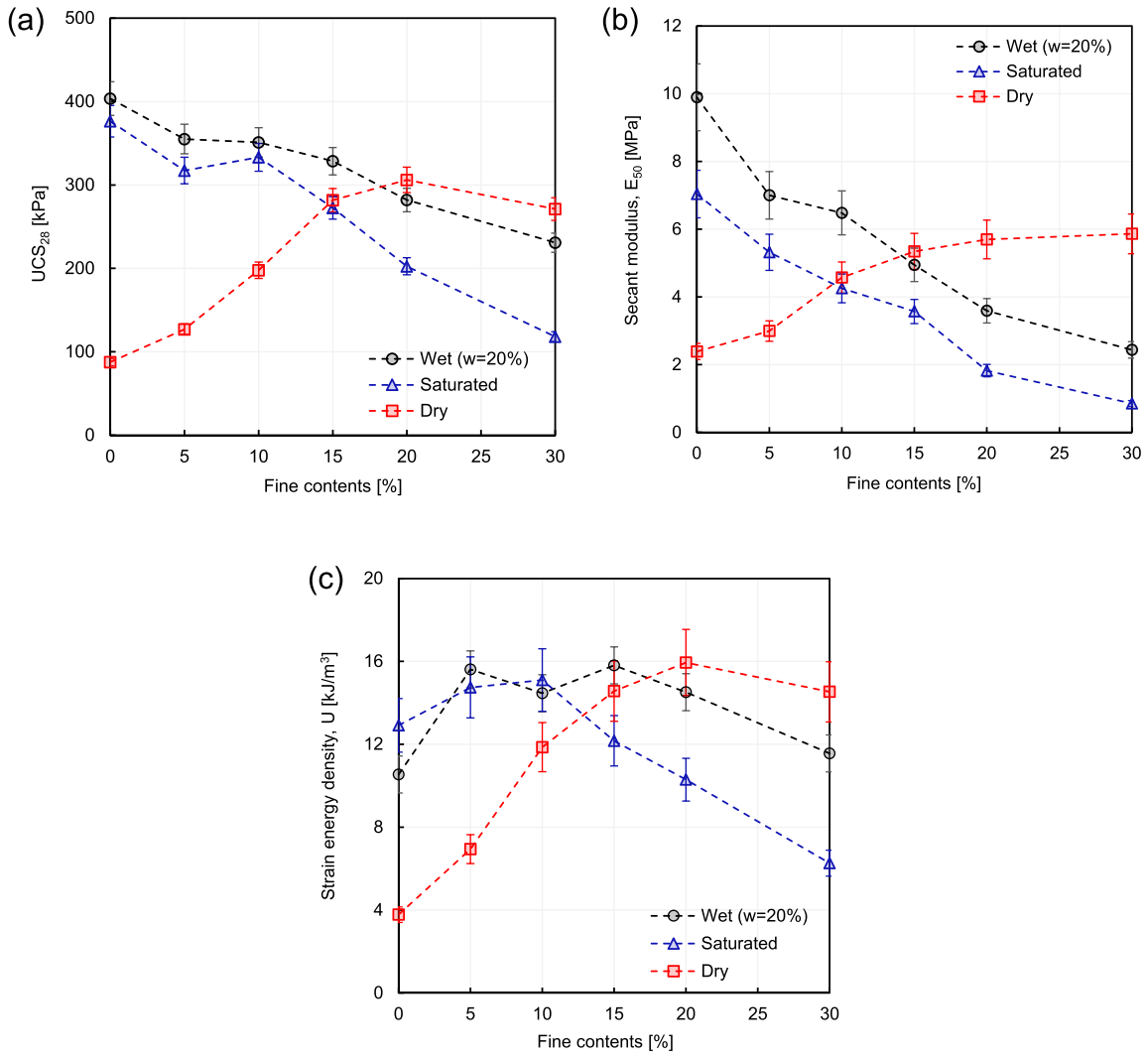

Fig. 8. Effect of fine contents on strength parameters; (a) UCS_{28}, (b) E_{50}, and (c) U.

Table 4
28-day UCS of CrXG-treated soil depending on soil composition and curing conditions.

	Wet-cured		Saturated-cured		Dry-cured	
Label	UCS_{28} [kPa]	Relative strength [%]	UCS_{28} [kPa]	Relative strength [%]	UCS_{28} [kPa]	Relative strength [%]
CSM_0	403.5	100	376.4	100	87.5	100
CSM_5	355.0	88.0	317.3	84.3	127.0	145.1
CSM_{10}	351.1	87.0	333.1	88.4	197.8	226.1
CSM_{15}	328.5	81.4	272.5	72.4	281.7	321.9
CSM_{20}	281.9	69.9	202.5	53.8	306.0	349.7
CSM_{30}	230.7	57.25	118.1	31.4	271.1	309.8

(1) fine-grained soil's inhibited of Cr^{3+}-crosslinking-induced gelation, and (2) the inter-granular void was filled with the CrXG-clay matrix, which had a greater water absorption capacity. Due to the competitive adsorption for Cr^{3+} between the XG hydrogel side chains and anionically-charged clay surfaces in the presence of water [35,58], clay particles probably disturbed crosslinking-induced gelation between XG and Cr^{3+} to occur, leading to a reduction in the crosslinking rate and crosslink density of the hydrogel and an increase in the gel strength [59]. Specifically, a higher fine content in the CSMs increases the likelihood of Cr^{3+} adsorption by the charged clay surface, thus, resulting in a greater decrease in strength and stiffness. This disturbance effect of clay particles was also reported in the crosslinking polymerization reactions of other polymers, such as chitosan [60], and polyacrylamide [59]. Furthermore, the lower crosslink density resulted in a higher soluble fraction (residual XG monomer) in the CrXG hydrogel. Thus, an increased number of both clay particles and residual XG monomers in the CrXG-clay matrix that filled the inter-granular voids exhibited a greater water absorption capacity, potentially weakening of inter-particle connections and reducing the strength and stiffness.

Furthermore, it is interesting to note that the strain energy density of wet- and saturated-cured samples increased with up to 10–15 % fine content before decreasing (Fig. 8c). The strain energy density is the amount of energy required to deform soil by breaking inter-particle bonds between soil grains [50]; thus, these results indicates that the addition of fines content allows for greater deformation of the CrXG–soil composite under loading until failure. As the fine content increased, the inter-granular void filling with the CrXG-clay matrix probably enhanced the packing state of the binary soil mixture. The strain energy density decreased after a fine content of 20 % because it exceeded the critical fine content threshold [61], where clay-filled voids surrounding sand grains acted as lubricants for sand particle sliding, decreasing the strength and strain energy density [62,63].

The dry-cured samples exhibited an increase of peak stress and failure strain in the stress-strain curve (Fig. 7c), showing the variation of

all strength parameters with an increasing fine content (Fig. 8). Notably, for a lower fine content (CSM_0 and CSM_5), the strength parameters of the dry-cured samples were smaller than those of the wet- and saturated-cured samples, whereas they were greater for a higher fine content (CSM_{20} and CSM_{30}). As noted in Section 3.1, for dry-cured CSM_0, dehydration condensed CrXG hydrogel into the film before a sufficient Cr^{3+} crosslinking reaction occurred, which led to the shrinkage-induced deterioration of the inter-granular connectivity in pure sand with a lower strength and stiffness [35]. Meanwhile, as the soil composition became well-graded with increasing fine content, the formation of dehydrated biopolymer-clay matrices within the sand particles enhanced contact coordination, providing artificial inter-granular cohesion [62], resulting in greater strength compared to wet- and saturated-cured samples.

Fig. 9 shows the difference between the maximum and minimum values of UCS_{28} and E_{50} (ΔUCS_{28} and ΔE_{50}) for the three curing methods by fine content. For the pure sand (CSM_0), the differences in UCS_{28} and E_{50} across the curing methods were approximately 300 kPa and 7.5 MPa, respectively. These differences decreased to 61 kPa and 1.8 MPa, respectively, at a fine content of 15 %, and increased to 176 kPa and 5 MPa, respectively, at a fine content of 30 %. Considering the various curing environments in geotechnical practices, ensuring consistent strength performance is crucial. Therefore, CSM_{15}, which had the most stable strength performance under the three curing conditions, was determined to be the optimal soil composition for CrXG–soil treatment and further durability assessment.

3.3. Strength durability under cyclic D-W condition

The strength durability of CrXG-treated CSM_0 and CSM_{15} under accelerated weathering conditions was investigated. Fig. 10 shows the variations in the density, UCS, and E_{50} of CrXG-treated CSM_0 and CSM_{15} exposed to laboratory cyclic D-W conditions. The values on the y-axis corresponding to cycle zero for samples wet-cured for two days. The UCS and E_{50} of CSM_0 decreased by 88.7 % (from 307 to 35 kPa) and 88.2 % (from 6.8 to 0.8 MPa), respectively, after the first cycle, followed by a slight further decrease, and stabilizing at a 93 % reduction in both UCS and E_{50} after the eighth (Figs. 10a and 10b). The significant reduction of UCS and E_{50} after the first drying process and a further slight reduction with the wetting process is related to the irreversible conversion of the rigid CrXG hydrogel to a film [35]. Once dried, the ability of the CrXG film to absorb water is reduced due to hydrophilic carboxyl groups being

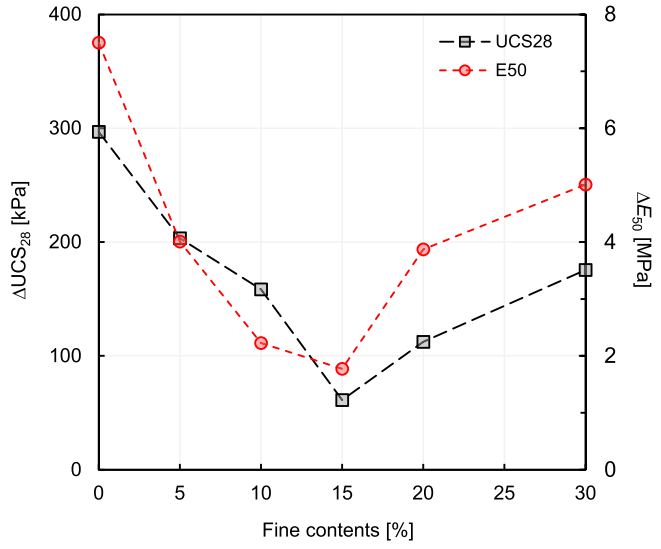

Fig. 9. Strength and stiffness differences among curing methods at each fine content.

predominantly occupied by cations. Thus, the strength and stiffness cannot recover to initial values (at cycle zero), but experience further reduction in the rewetting process, probably due to the partial softening of the biopolymer gel in continuous water exposure [56]. In contrast, the UCS and E_{50} of CSM_{15} decreased by 61.9 % (258–99 kPa) and 61.3 % (3.2–1.3 %), respectively, after the first cycle. Subsequent cycles showed a slight further decrease similar to CSM_0, and UCS and E_{50} finally reduced by 69.7 % and 72.2 %, respectively, after the eighth cycle. Although the strength and stiffness after wetting were smaller compared to the initial state (zero cycle), the dry strength showed resilience after the overall D-W cycle due to dehydrated biopolymer-clay matrices, as noted in Section 3.2. The strength and stiffness recovered to over 300 kPa and 5 MPa, respectively, after each drying process.

Moreover, it is important to note that both the CrXG-treated CSM_0 and CSM_{15} samples exhibited only a 1.5 % density variation between the first and eighth cycles under all wetting and drying conditions. This contrasts with the structural disturbance and density reduction observed in previous works on cyclic D-W responses of un-crosslinked XG-treated sand-fine mixtures [32,64]. Thus, it can be concluded that CrXG-treated soils demonstrate better resistance to cyclic D-W weathering compared to conventional XG-treated soils. In particular, CrXG-treated CSM15 maintains its dry strength performance.

3.4. Long-term strength and water content change under atmospheric weathering condition

The long-term strengths of CrXG-treated CSM_0 and CSM_{15} under in-situ weathering conditions were investigated by exposing the samples outdoors for 130 days. Fig. 11 shows the soil mass loss and the changes in UCS and water content of CrXG-treated CSM_0 and CSM_{15} with temperature variations and precipitation at the test site during the experiment. The soil mass loss was calculated from the weight change relative to the initial dry weight of each sample. The cumulative mass loss due to weathering increased over time, reaching 2.9 % for CSM_0 and 2.5 % for CSM_{15} after 130 days of exposure (Fig. 11b).

For the CSM_0 samples, both the UCS and water content decreased with changing atmospheric conditions from an initial UCS of 249 kPa to a water content of 20 %. After 28 days, the UCS retained 47 % of its initial strength, and only 20 % of its initial strength was maintained after 42 days (Fig. 11c). When the water content increased from ~1–14.2 % at 67 days due to rainfall at 65 days (Fig. 11a), the UCS degraded to 34 kPa (87 % reduction compared to the initial values) and was maintained below 100 kPa. This finding corresponds to laboratory D-W test results, where CSM_0 samples experienced a strength reduction upon dehydration and did not recover their strength after rewetting.

The CSM_{15} samples showed less UCS degradation over a month (from 371 to 331 kPa, 11 %) than CSM_0 (from 249 to 117 kPa, 53 %). 64 % of the initial strength was retained even after 56 days of exposure (Fig. 11d). The lowest UCS (121 kPa) and highest water content (12.9 %) were observed at 67 days, similar to CSM_0. However, it is interesting to note that UCS increased again up to 300 kPa with dehydration due to the durable aggregation effect of the CrXG-clay matrices, as observed in the laboratory D-W tests.

The outdoor durability test results demonstrate that CSM_{15} is more resilient and erosion-resistant to in-situ weathering conditions, including rainfall and temperature variations, suggesting that CrXG–soil stabilization with 15 % fine content has the potential for applications in geotechnical practices, such as slope surface protection.

3.5. SEM and ESEM microscopic analysis of weathered CrXG-treated CSMs

To elucidate the distinct microstructural characteristics of the D-W processes, the microstructures of CSM_0 and CSM_{15} were analyzed. Fig. 12 shows the SEM and ESEM images of the CrXG-treated soils after the first and eighth cycles of the D-W process.

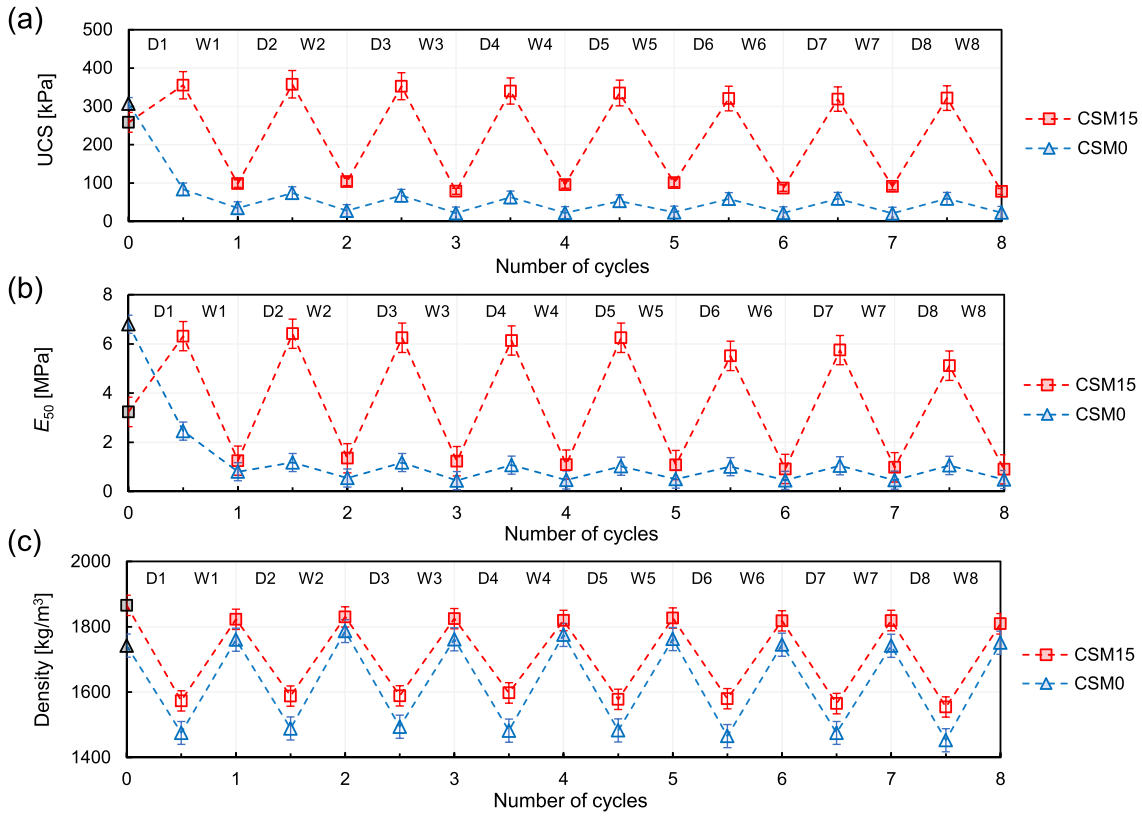

Fig. 10. Results of cyclic D-W durability test for CSM_0 and CSM_{15}. Variations of (a) density, (b) UCS, and (c) E_{50} by cycles.

For the CSM_0 samples, when dried, the CrXG hydrogel in the pores transitioned into a thin CrXG film, creating particle coatings and bridges between the grains and resulting in larger pore spaces (Fig. 12a). Upon rewetting, the CrXG film did not swell, and the fissured CrXG film from dehydration did not recover (Fig. 12b). This characteristic allowed more water intrusion upon rewetting, causing a slight increase in density (Fig. 10c) and irreversible strength and stiffness reduction (Fig. 10a and b) after the first drying process. After the eighth D-W cycles, the CSM_0 samples exhibited disconnected and detached CrXG films due to weathering (Fig. 12c and d). The loss of inter-particle contact contributed to the gradual decrease in the UCS as the number of cycles increased (Fig. 10a).

In the case of CSM_{15} samples, CrXG-clay matrices, which are thicker than the CrXG film, were observed between sand grains, showing smaller pore spaces compared to CSM_0 (Fig. 12e). The CrXG-clay matrices enhanced contact coordination and inter-granular cohesion, resulting in an increased UCS, E_{50}, and U (Fig. 8). Upon rewetting, the exterior of the CrXG-clay matrices swelled slightly because of the free XG and clay particles (Fig. 12f), but did not exhibit disturbances from the swelling-induced volume expansion observed in pure XG-treated clay [65]. After eight D-W cycles, the particle coatings and bridges formed by the CrXG-clay matrices were less disturbed compared to CSM_0 (Fig. 12f), which is consistent with the improved durability observed in both the indoor and outdoor durability tests.

3.6. FTIR spectra analysis for weathered CrXG-treated CSMs

Fig. 13 compares the FTIR spectra of CrXG-treated CSM0 and CSM15 with those treated with pure XG. The spectra of pure XG-treated CSM_0 showed characteristic absorption peaks corresponding to various functional groups: hydrogen-bonded O-H stretching at 3378 cm^{-1}, methylene C-H stretching at 2915 cm^{-1}, C═O stretching of acetyl groups at 1720 cm^{-1}, asymmetrical stretching of -COO^- of pyruvate groups at 1620 cm^{-1}, symmetrical stretching of -COO^- of glucuronic acid at 1400 cm^{-1}, and C-O-C stretching of ether groups at 1022 cm^{-1}. [66–69]. Upon crosslinking XG with Cr^{3+} and undergoing cyclic D-W processes, notable shifts in these absorption peaks were observed (Fig. 13a). The respective absorption peaks shifted to 3405, 2935, 1724, 1627, and 1068 cm^{-1} after crosslinking, with a shift to higher wavenumbers (i.e., red shift) attributed to the metal coordination between Cr^{3+} and the carboxyl (–COO) and hydroxyl (–OH) groups [70]. This coordination is crucial as it inhibited the dissolution of submerged XG, typically occurring at the carboxyl groups [71], thus preventing reactivation of the XG polymer in water exposed conditions. After enduring eight D-W cycles, the respective absorption peaks reverted or blue-shifted to 3394, 2927, 1720, 1608, and 1033 cm^{-1}, suggesting a weakening or breakdown of the Cr^{3+} and XG bonds due to the cyclic weathering conditions. Additionally, the narrowing of the peak area between 3000–3700 cm^{-1}, which represents hydrogen-bonded O-H stretching, signals a reduction in strength and an increase in hygroscopicity of the CrXG gel [72].

For CSM_{15} samples, similar absorption peaks were observed at 2927, 1720, 1635, and 1018 cm^{-1}, corresponding to the methylene C-H stretching, C═O stretching of acetyl groups, asymmetrical stretching of -COO^- of pyruvate groups, symmetrical stretching of -COO^- of glucuronic acid, and C-O-C stretching of ether groups, respectively. An absorption band near 3621 cm^{-1} denotes the outer and inner -OH groups of the ordered structure of kaolinite [73]. Cr^{3+}-crosslinking shifted the absorption peak at the C-H stretching of methylene groups from 2927 to 2939 cm^{-1}, suggesting coordination between the acetyl groups and Cr^{3+}, which remained constant throughout the D-W cycles. The minimal variation in the absorption peaks at 3621, 1720, 1636, and 1018 cm^{-1} during the D-W cycles indicates more stable associations in CSM_{15}, aligned with the improved strength durability of the CSM_{15} samples.

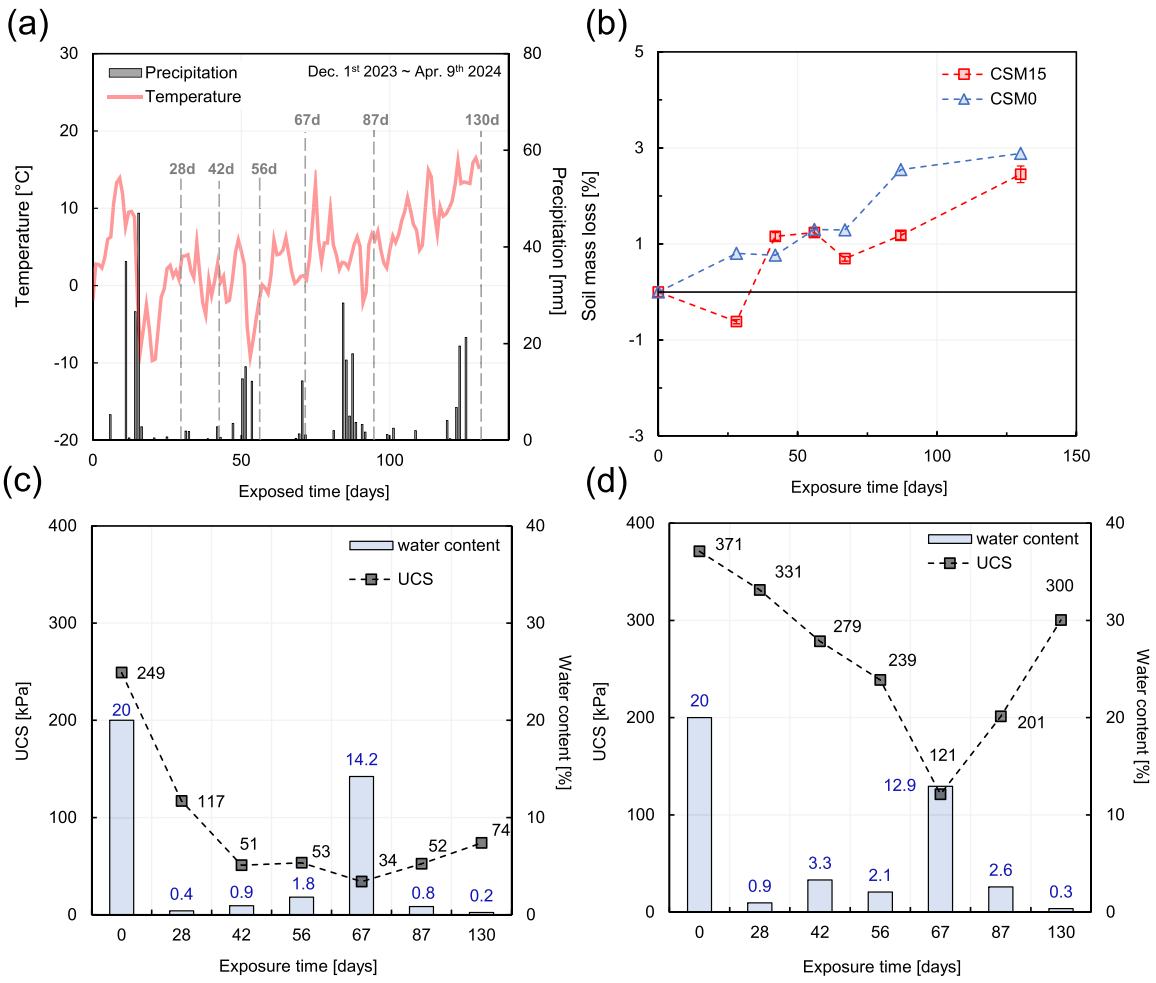

Fig. 11. Results of atmospheric weathering durability test for CSM_0 and CSM_{15}; (a) temperature variations and precipitation in test site during experiment, (b) soil mass loss in percent, (c) UCS and water content of CSM_0, and (d) UCS and water content of CSM_{15}.

4. Discussion

4.1. Use of the hyperbolic model to estimate long-term UCS of CSMs

The nonlinear development of the UCS of the CSMs with the curing time (Fig. 6) was analyzed using the hyperbolic model, which is widely used for cement-based materials [74,75].

$$UCS = UCS_{ult} \times \frac{kt}{1 + kt} = \frac{t}{\frac{1}{k \times UCS_{ult}} + \frac{t}{UCS_{ult}}} \quad (2)$$

where UCS_{ult} is the ultimate UCS, t is the curing time, and k is the rate factor capturing the initial slope between the UCS and t. The hyperbolic coefficients in Eq. (2) were determined using the method of Duncan and Chang [74]. Table 5 summarizes the hyperbolic coefficients of the CSMs samples. Fig. 14 depicts a representative fitting result for wet-cured CSM_{15}, showing the measured UCS and estimated UCS_{ult}.

The general XG-Cr^{3+}-crosslinking process was characterized by two stages: (1) an early rise due to the initiation of reactions between Cr^{3+} and XG, and (2) a subsequent stagnation stage related to the completion of a three-dimensional polymer network formation in the CrXG gel [76]. Thus, the UCS variation with curing time in most CrXG-treated CSMs fits the hyperbolic model well, such as for cement-treated soil [75], with a high coefficient of determination ($R^2 > 0.9$). However, the poor model fit ($R^2 < 0.4$) for saturated-cured CSM_{30} and dry-cured CSM_0 indicated no clear time-dependent development of UCS under these conditions, as described in Section 3.1.

Fig. 15 shows the changes in k values with the fine content in the CSMs. Under wet- and saturated-cured conditions, k generally increased with fine content, reflecting a decrease in the required curing time for the completion of the gelation process in CSMs with more fine-grained soils. Thus, it can be inferred that fine-grained soil in wet- and saturated-cured samples inhibited XG binding with Cr^{3+} and promoted XG-Cr^{3+}-crosslinking. Specifically, the infiltration of free water during saturated-curing accelerated the mitigation of XG-Cr binding, leading to a higher k increase at 10 %–20 % fine content.

In dry-cured samples, the high k values for CSM_5 and CSM_{10} were related to small UCS changes between UCS_1 and UCS_{28}. As the fine content increased, UCS_{28} increased due to the formation of dehydrated biopolymer-clay matrices within the sand particles providing inter-granular cohesion. This led to a lower k value. Nevertheless, this does not imply that an increased curing time is required to reach the ultimate strength because there was no apparent time-dependent strengthening effect by gelation in the dry-cured samples.

Through a hyperbolic model analysis, it was confirmed that the measured and predicted UCS values aligned well within a maximum error of 7.8 %. The hyperbolic model with coefficients obtained from the 28 day test results was sufficient to predict the long-term UCS of the stabilized soil [75]. Therefore, the UCS prediction model and estimated UCS_{ult} can be utilized to design CrXG–soil stabilization, considering the strength required in geotechnical engineering practices. However, it should be noted that UCS may degrade depending on the weathering conditions, as discussed in Sections 3.3 and 3.4.

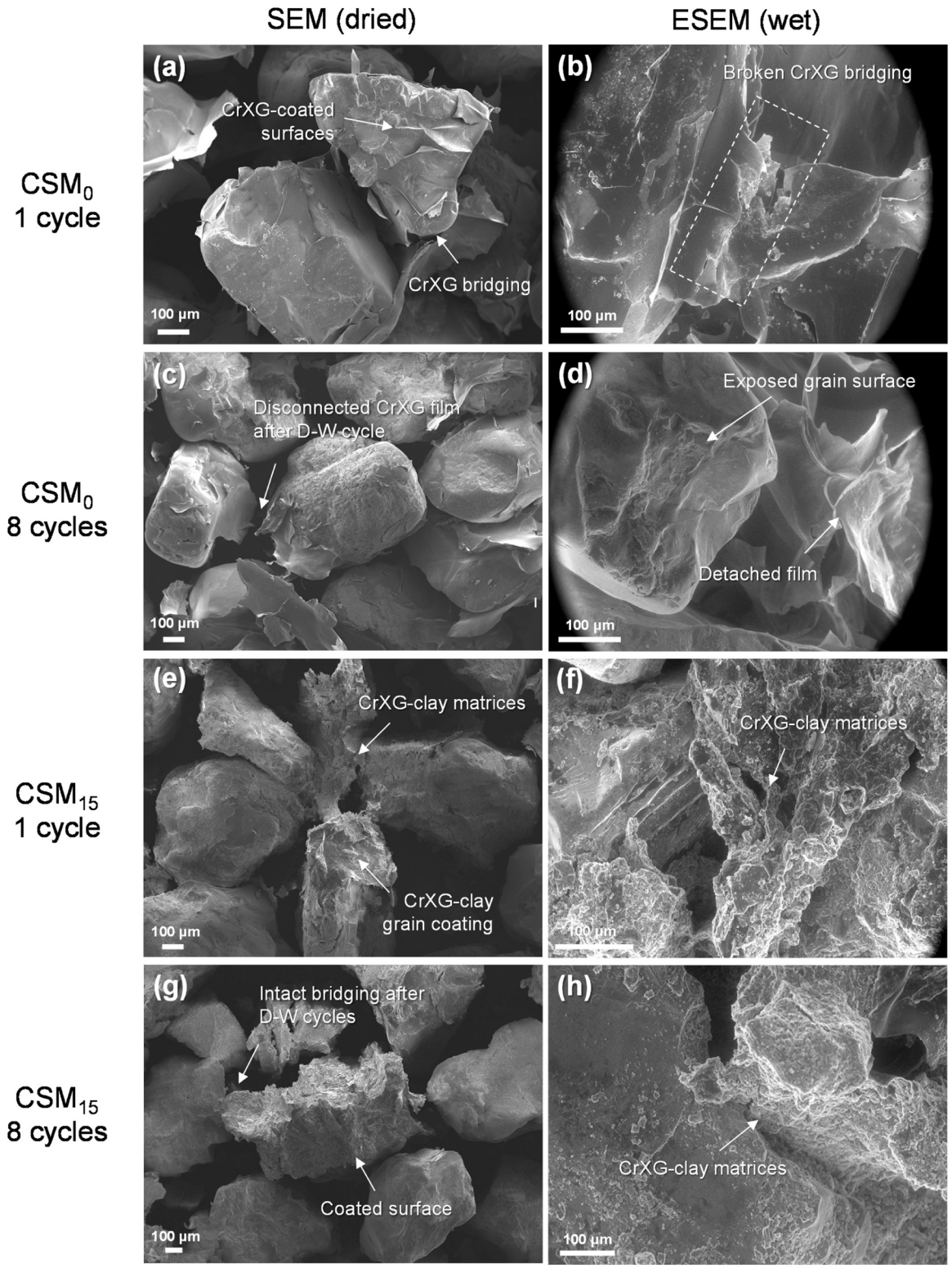

Fig. 12. SEM and ESEM images: (a and b) CSM_0 after 1 cycle, (c and d) CSM_0 after 8 cycles, (e and f) CSM_{15} after 1 cycle, and (g and h) CSM_{15} after 8 cycles.

4.2. Durability index and comparison with other biopolymers

To compare the durability of the CrXG-treated CSM with other biopolymer-stabilized soil composites under cyclic D-W conditions, the durability index (DI) was determined using Eq. 3 [77]:

$$DI[\%] = \frac{UCS_{Ncyc}}{UCS_{1cyc}} \times 100 \quad (3)$$

where UCS_{Ncyc} is the UCS after N cycles of D–W and UCS_{1cyc} is the initial UCS in the first cycle.

Fig. 16 presents the logarithmic trend of the DI values over D-W cycles for 1 % CrXG-treated CSMs, 1 % lignin-treated clayey sand (SC), 2 % XG-starch compound-treated SC, and 1 % XG-treated silty sand (SM) [32,64,78]. The CrXG treatment exhibited improved strength durability, maintaining a DI of over 71 % for CSM_0 and over 90 % for

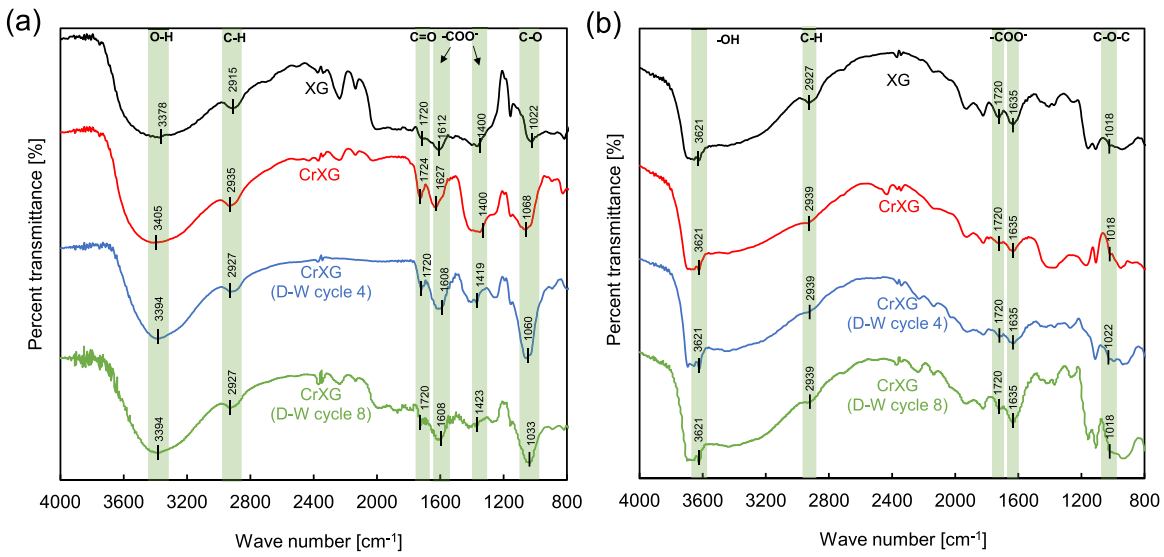

Fig. 13. FTIR spectra of weathered CrXG-soil composite in comparison to intact XG- and CrXG-soil composite; (a) CSM_0, and (b) CSM_{15}.

Table 5
Hyperbolic model coefficients for UCS of CrXG-treated soils.

	Estimated UCS_{ult} [kPa]			Rate factor, k [1/day]			R^2 of fit		
Label	Wet	Saturated	Dry	Wet	Saturated	Dry	Wet	Saturated	Dry
CSM_0	382	297	-	6.715	9.377	-	0.999	0.985	0.108
CSM_5	332	331	128	7.723	7.744	40.030	0.996	0.997	0.799
CSM_{10}	346	328	187	12.107	13.115	39.079	0.999	0.997	0.928
CSM_{15}	322	261	282	12.136	16.939	14.929	0.999	0.978	0.988
CSM_{20}	268	215	327	18.044	27.311	13.003	0.990	0.904	0.994
CSM_{30}	222	-	265	33.937	-	23.102	0.913	0.339	0.964

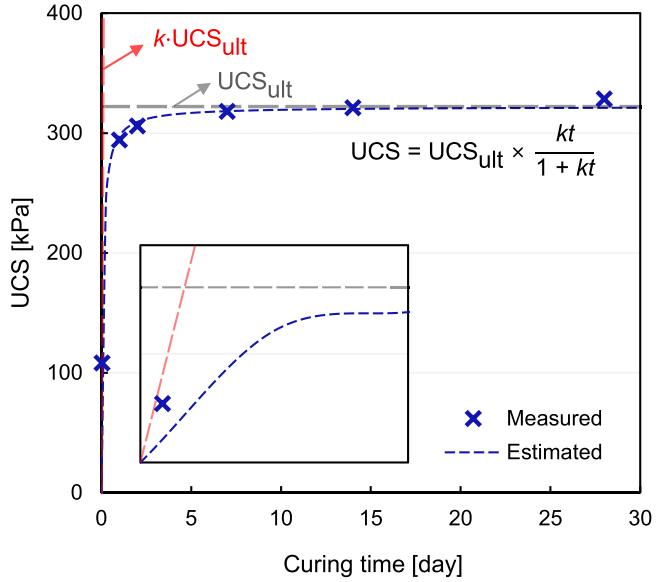

Fig. 14. Hyperbolic model for capturing the nonlinear development of UCS with curing time.

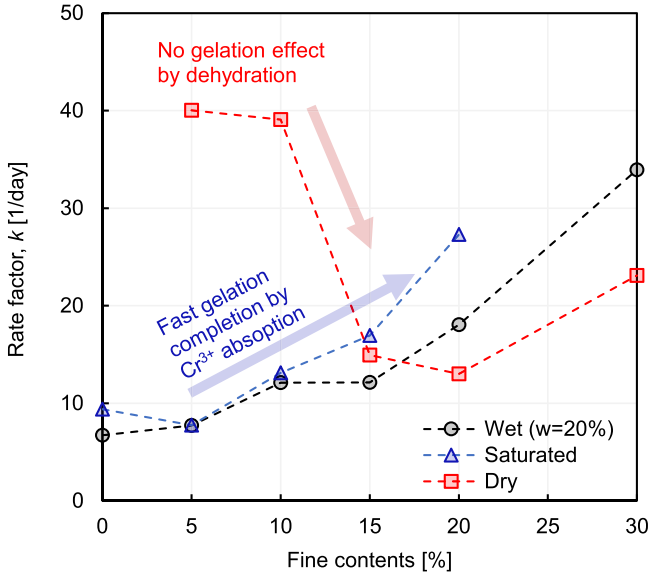

Fig. 15. Hyperbolic coefficient changes with fine content in CrXG-soil composites.

CSM_{15}. Although the CSM_0 samples exhibited a decrease in strength during the first cycle, they subsequently maintained their strength. Conversely, the CSM_{15} samples exhibited an increase in UCS after the initial drying and maintained adequate strength throughout the cycles, demonstrating their improvement over other BP-treated samples. Pure XG- and XG-starch-treated soil samples exhibited relatively poor DI owing to the hydrophilic characteristics of XG, leading to severe swelling upon exposure to moisture and loosening of the soil matrix [79]. Interestingly, lignin, which has both hydrophilic and hydrophobic side chains, exhibited strength retention comparable to that of CrXG-treated CSM_0. This was attributed to the ability of lignin to reattach to soil particles and partially restore broken cracks upon the

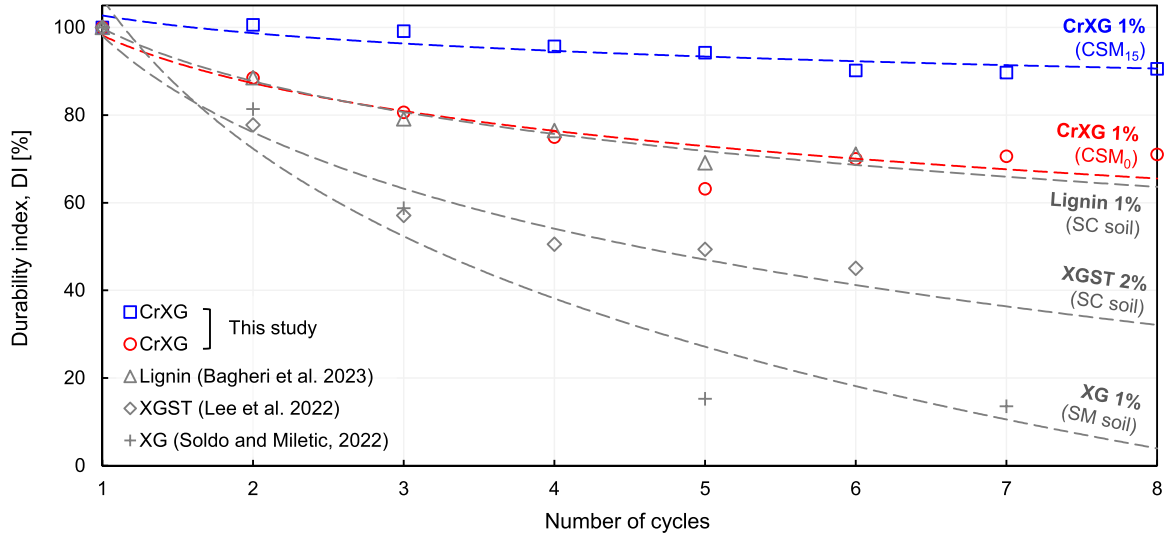

Fig. 16. Durability index and comparison with other biopolymer-soil composites.

re-dehydration of submerged samples, thereby maintaining strength [78]. These results indicate that the formation of CrXG-clay matrices in soil with the addition of 15 % fine content provides stable and competitive strength retention under weathering conditions compared to other biopolymer stabilizers, suggesting their potential for geotechnical engineering applications.

4.3. Implications and limitations

The results of this study demonstrate that a sand-to-clay ratio of 85:15 is promising for ensuring consistent strength performance in CrXG soil stabilization. This mixture also maintained superior strength and durability compared with other biopolymer stabilizers. For practical applications, CrXG-treated CSM_{15} composites can be utilized for slope surface protection in earthen structures, such as levees or bridge abutments, thereby enhancing the surface erosion resistance and surface hardness [30]. Based on the site application case studies of XG-based compound biopolymers [80,81], direct compaction and pressurized spraying methods can be similarly utilized for CrXG-treated CSM_{15} composites. However, further investigations are required to validate the homogeneity in the field mixing condition and the corresponding strength performance of the implemented CrXG-soil composites. Additionally, research utilizing naturally occurring soils (i.e., weathered soil) from sites of interest is also required to evaluate the applicability of CrXG-treated CSM_{15} composites in different soil conditions. These factors significantly affect workability, including pumping efficiency, adhesion capabilities of the slope surface, and post-construction strength performance [47,82,83].

5. Conclusions

This study conducted extensive mechanistic and microscopic investigations to address the significant gaps in understanding the effects of the curing time (0.04–28 days), curing conditions (wet, saturated, and dry), and soil composition (fine contents from 0 % to 30 %) on the strength and durability of CrXG–soil composites. The results are instrumental for designing optimal soil compositions for CrXG-treated CSMs, particularly for field applications such as slope surface protection. This study also proposed a long-term strength prediction model for these composites. The key findings are summarized as follows:

- The curing environment profoundly influenced the strength development of CrXG-treated soils. A nonlinear increase in UCS over time regardless of the fine content was observed in both wet- and saturated-cured samples, attributed to the time-dependent evolution of CrXG gel strength. Conversely, dry-cured samples showed minimal strength development, hindered by early-stage dehydration-induced condensation of the polymer, which restricted further cation-crosslinking.
- The fine content significantly altered the strength behavior depending on the curing condition. Increasing the fine content made wet- and saturated-cured samples more ductile. This reduced the UCS and E_{50} due to clay particles interfering with Cr^{3+}-crosslinking-induced gelation and synergetic water absorption by filling inter-granular voids with CrXG-clay matrix. However, in dry-cured samples, increasing fine content enhanced both UCS and E_{50} due to the formation of dehydrated biopolymer-clay matrices within the sand particles, enhancing contact coordination and providing inter-granular cohesion.
- CSM_{15} demonstrated the most consistent strength performance across all curing environments, exhibiting minimal structural disturbances and greater resilience against both controlled and in-situ weathering conditions. SEM and FTIR analyses confirmed the more stable inter-granular connectivity in CSM_{15} after weathering, supporting the observed strength durability.
- A hyperbolic model was introduced to predict the time-dependent development of UCS in CrXG-treated CSMs. The correlation between measured and predicted UCS values was notably close, with a maximum error of 7.8 %. This UCS prediction model and the estimated ultimate UCS can guide the design of CrXG–soil stabilization, considering the required strength in geotechnical engineering applications.

While this study focused on a specific biopolymer content and type, the findings elucidate the complex interactions among biopolymers, clay, and crosslinked-cations, enhancing our understanding of the soil strengthening efficiency of CrXG–soil stabilization across different soil compositions and curing conditions. This research highlights the potential of CrXG–soil composites as a sustainable surface protection material for earthen structures, including levees and bridge abutments, by proposing optimal soil compositions and a robust long-term strength prediction model. Future studies are recommended to explore in-situ mixing homogeneity and the application of naturally occurring soils to enhance field applicability.

CRediT authorship contribution statement

Jeong-Uk Bang: Methodology, Investigation, Data curation, Formal analysis, Visualization, Writing - original draft. **Minhyeong Lee:** Conceptualization, Methodology, Data curation, Formal analysis, Visualization, Supervision, Writing - original draft, Writing - review and editing. **Dong-Yeup Park:** Investigation. **Ilhan Chang:** Supervision, Writing - review and editing. **Gye-Chun Cho:** Supervision, Project administration, Funding acquisition.

Declaration of Competing Interest

The authors declare that they have no known competing financial interests or personal relationships that could have appeared to influence the work reported in this paper.

Data availability

Data will be made available on request.

Acknowledgements

This work was supported by the National Research Foundation of Korea (NRF) grant funded by the Korea government (MSIT) (2023R1A2C300559611) and the Ministry of Oceans and Fisheries (MOF) of the Korean Government (No. 20220364).

References

[1] A. Collison, S. Wade, J. Griffiths, M. Dehn, Modelling the impact of predicted climate change on landslide frequency and magnitude in SE England, Eng. Geol. 55 (3) (2000) 205–218, https://doi.org/10.1016/S0013-7952(99)00121-0.
[2] C. Wenger, Better use and management of levees: reducing flood risk in a changing climate, Environ. Rev. 23 (2) (2015) 240–255, https://doi.org/10.1139/er-2014-0060.
[3] A. Toimil, I.J. Losada, P. Camus, P. Díaz-Simal, Managing coastal erosion under climate change at the regional scale, Coast. Eng. 128 (2017) 106–122, https://doi.org/10.1016/j.coastaleng.2017.08.004.
[4] T. Chompoorat, T. Thepumong, A. Khamplod, S. Likitlersuang, Improving mechanical properties and shrinkage cracking characteristics of soft clay in deep soil mixing, Const. Build. Mater. 316 (2022) 125858, https://doi.org/10.1016/j.conbuildmat.2021.125858.
[5] T. Chompoorat, K. Thanawong, S. Likitlersuang, Swell-shrink behaviour of cement with fly ash-stabilised lakebed sediment, Bull. Eng. Geol. Environ. 80 (2021) 2617–2628, https://doi.org/10.1007/s10064-020-02069-2.
[6] J.M. Manso, V. Ortega-López, J.A. Polanco, J. Setién, The use of ladle furnace slag in soil stabilization, Constr. Build. Mater. 40 (2013) 126–134, https://doi.org/10.1016/j.conbuildmat.2012.09.079.
[7] A.A. Firoozi, C.G. Olgun, A.A. Firoozi, M.S. Baghini, Fundamentals of soil stabilization, Int. J. Geo Eng. 8 (1) (2017) 1–16, https://doi.org/10.1186/s40703-017-0064-9.
[8] L. Barcelo, J. Kline, G. Walenta, E. Gartner, Cement and carbon emissions, Mat. Struct. 47 (6) (2014) 1055–1065, https://doi.org/10.1617/s11527-013-0114-5.
[9] R.B. Kogbara, A review of the mechanical and leaching performance of stabilized/solidified contaminated soils, Environ. Rev. 22 (1) (2014) 66–86, https://doi.org/10.1139/er-2013-0004.
[10] J.K. Mitchell, J.C. Santamarina, Biological considerations in geotechnical engineering, J. Geotech. Geoenviron. Eng. 131 (10) (2005) 1222–1233, https://doi.org/10.1061/(ASCE)1090-0241(2005)131:10(1222).
[11] I. Chang, J. Im, G.-C. Cho, Introduction of microbial biopolymers in soil treatment for future environmentally-friendly and sustainable geotechnical engineering, Sustainability 8 (3) (2016), https://doi.org/10.3390/su8030251.
[12] E. Worrell, L. Price, N. Martin, C. Hendriks, L.O. Meida, Carbon dioxide emissions from the global cement industry, Ann. Rev. Energy Environ. 26 (1) (2001) 303–329, https://doi.org/10.1146/annurev.energy.26.1.303.
[13] I. Chang, J. Im, A.K. Prasidhi, G.-C. Cho, Effects of xanthan gum biopolymer on soil strengthening, Const. Build. Mater. 74 (2015) 65–72, https://doi.org/10.1016/j.conbuildmat.2014.10.026.
[14] R.A. Nugent, G. Zhang, R.P. Gambrell, Effect of exopolymers on the liquid limit of clays and its engineering implications, Trans. Res. Rec. 2101 (1) (2009) 34–43, https://doi.org/10.3141/2101-05.
[15] I. Chang, Y.-M. Kwon, G.-C. Cho, Effect of pore–fluid chemistry on the undrained shear strength of xanthan gum biopolymer-treated clays, J. Geotech. Geoenviron. Eng. 147 (11) (2021) 06021013, https://doi.org/10.1061/(ASCE)GT.1943-5606.0002652.
[16] Y.-M. Kwon, I. Chang, G.-C. Cho, Xanthan biopolymer-based soil treatment effect on kaolinite clay fabric and structure using XRD analysis, Sci. Rep. 13 (1) (2023) 11666, https://doi.org/10.1038/s41598-023-38844-w.
[17] S.-G. Choi, I. Chang, M. Lee, J.-H. Lee, J.-T. Han, T.-H. Kwon, Review on geotechnical engineering properties of sands treated by microbially induced calcium carbonate precipitation (MICP) and biopolymers, Const. Build. Mater. 246 (2020) 118415, https://doi.org/10.1016/j.conbuildmat.2020.118415.
[18] K. Lemboye, A. Almajed, Effect of varying curing conditions on the strength of biopolymer modified sand, Polymers 15 (7) (2023) 1678, https://doi.org/10.3390/polym15071678.
[19] J.-E. Ryou, J.Y. Lee, W.-T. Hong, B. Yang, J. Jung, Effects of curing and soil type on unconfined compressive strengths and hydraulic conductivities of thermo-gelation biopolymer treated soils, Constr. Build. Mater. 432 (2024) 136493, https://doi.org/10.1016/j.conbuildmat.2024.136493.
[20] Z. Chen, J. Liu, Y. Wang, C. Qi, X. Ma, W. Che, K. Ma, Wetting–drying effects on the mechanical performance of xanthan gum biopolymer-stabilized soil, Environ. Earth Sci. 83 (7) (2024) 197, https://doi.org/10.1007/s12665-024-11483-8.
[21] M. Hamza, Z. Nie, M. Aziz, N. Ijaz, M.F. Ameer, Z. Ijaz, Geotechnical properties of problematic expansive subgrade stabilized with xanthan gum biopolymer, Road. Mater. Pavement Des. 24 (7) (2023) 1869–1883, https://doi.org/10.1080/14680629.2022.2092027.
[22] S. Seo, M. Lee, J. Im, Y.-M. Kwon, M.-K. Chung, G.-C. Cho, I. Chang, Site application of biopolymer-based soil treatment (BPST) for slope surface protection: in-situ wet-spraying method and strengthening effect verification, Const. Build. Mater. 307 (2021) 124983, https://doi.org/10.1016/j.conbuildmat.2021.124983.
[23] I. Chang, J. Im, A.K. Prasidhi, G.C. Cho, Effects of xanthan gum biopolymer on soil strengthening, Constr. Build. Mater. 74 (2015) 65–72, https://doi.org/10.1016/j.conbuildmat.2014.10.026.
[24] A. Bouazza, W.P. Gates, P.G. Ranjith, Hydraulic conductivity of biopolymer-treated silty sand, Geotechnique 59 (1) (2009) 71–72, https://doi.org/10.1680/geot.2007.00137.
[25] A.F. Cabalar, M. Wiszniewski, Z. Skutnik, Effects of xanthan gum biopolymer on the permeability, odometer, unconfined compressive and triaxial shear behavior of a sand, Soil Mech. Found. Eng. 54 (5) (2017) 356–361, https://doi.org/10.1007/s11204-017-9481-1.
[26] Y.M. Kwon, S.M. Ham, T.H. Kwon, G.C. Cho, I. Chang, Surface-erosion behaviour of biopolymer-treated soils assessed by EFA, Geotech. Lett. 10 (2) (2020) 106–112, https://doi.org/10.1680/jgele.19.00106.
[27] I. Chang, A.K. Prasidhi, J. Im, H.D. Shin, G.C. Cho, Soil treatment using microbial biopolymers for anti-desertification purposes, Geoderma 253 (2015) 39–47, https://doi.org/10.1016/j.geoderma.2015.04.006.
[28] T.P.A. Tran, G.-C. Cho, C. Ilhan, Water retention characteristics of biopolymer hydrogel containing sandy soils, Hue Univ. J. Sci. Earth Sci. Environ. 129 (4A) (2020), https://doi.org/10.26459/hueuni-jese.v129i4A.5652.
[29] W. Kang, D. Ko, J. Kang, Erosion resistance performance of surface-reinforced levees using novel biopolymers investigated via real-scale overtopping experiments, Water 13 (18) (2021) 2482, https://doi.org/10.3390/w13182482.
[30] M. Lee, I. Chang, S.-J. Kang, D.-H. Lee, G.-C. Cho, Alkaline induced-cation crosslinking biopolymer soil treatment and field implementation for slope surface protection, Geomech. Eng. 33 (1) (2023) 29–40, https://doi.org/10.12989/gae.2023.33.1.029.
[31] Y.-M. Kwon, J.-H. Moon, G.-C. Cho, Y.-U. Kim, I. Chang, Xanthan gum biopolymer-based soil treatment as a construction material to mitigate internal erosion of earthen embankment: a field-scale, Const. Build. Mater. 389 (2023) 131716, https://doi.org/10.1016/j.conbuildmat.2023.131716.
[32] M. Lee, Y.M. Kwon, D.Y. Park, I. Chang, G.C. Cho, Durability and strength degradation of xanthan gum based biopolymer treated soil subjected to severe weathering cycles, Sci. Rep. 12 (1) (2022) 19453, https://doi.org/10.1038/s41598-022-23823-4.
[33] J. Patel, B. Maji, N. Moorthy, S. Maiti, Xanthan gum derivatives: review of synthesis, properties and diverse applications, RSC Adv. 10 (45) (2020), 27103-27136, https://doi.org/10.1039%2Fd0ra04366d.
[34] H. Nolte, S. John, O. Smidsrod, B.T. Stokke, Gelation of xanthan with trivalent metal-ions, Carbohydr. Polym. 18 (4) (1992) 243–251, https://doi.org/10.1016/0144-8617(92)90089-9.
[35] M. Lee, I.L. Chang, G.C. Cho, Advanced biopolymer-based soil strengthening binder with trivalent chromium-xanthan gum crosslinking for wet strength and durability enhancement, J. Mater. Civ. Eng. 35 (10) (2023) 04023360, https://doi.org/10.1061/JMCEE7.MTENG-16123.
[36] M. Lee, I. Chang, D.Y. Park, G.C. Cho, Strengthening and permeability control in sand using Cr3+-crosslinked xanthan gum biopolymer treatment, Transp. Geotech. 43 (2023) 101122, https://doi.org/10.1016/j.trgeo.2023.101122.
[37] ASTM, Standard Test Method for Particle Size Distribution of Catalytic Materials by Laser Light Scattering, ASTM International, West Conshohocken, PA, 2020.
[38] ASTM, Standard Test Methods for Liquid Limit, Plastic Limit, and Plasticity Index of Soils, ASTM International, West Conshohocken, PA, 2018.
[39] E. Pelletier, C. Viebke, J. Meadows, P. Williams, A rheological study of the order–disorder conformational transition of xanthan gum, Biopolym. Org. Res. Biomol. 59 (5) (2001) 339–346, https://doi.org/10.1002/1097-0282(20011015)59:5<339::AID-BIP1031>3.0.CO;2-A.
[40] W.E. Rochefort, S. Middleman, Rheology of xanthan gum- salt, temperature, and strain effects in oscillatory and steady shear experiments, J. Rheol. 31 (4) (1987) 337–369, https://doi.org/10.1122/1.549953.
[41] ASTM, Standard Test Methods for Laboratory Determination of Water (Moisture) Content of Soil and Rock by Mass, ASTM International, West Conshohocken, PA, 2019.

[42] ASTM, Standard Test Methods for Particle-size Distribution (Gradation) of Soils Using Sieve Analysis, ASTM International, West Conshohocken, PA, 2017.
[43] ASTM, Standard Test Methods for Laboratory Compaction Characteristics of Soil Using Modified Effort (56,000 Ft-Lbf/Ft^3 (2,700 KN-m/m^3)), ASTM International, West Conshohocken, PA, 2021.
[44] ASTM, Standard Test Methods for Specific Gravity of Soil Solids by Water Pycnometer, ASTM International, West Conshohocken, PA, 2023.
[45] J. Ni, S.S. Li, L. Ma, X.Y. Geng, Performance of soils enhanced with eco-friendly biopolymers in unconfined compression strength tests and fatigue loading tests, Constr. Build. Mater. 263 (2020) 120039, https://doi.org/10.1016/j.conbuildmat.2020.120039.
[46] H. Fatehi, D.E.L. Ong, J. Yu, I. Chang, The effects of particle size distribution and moisture variation on mechanical strength of biopolymer-treated soil, Polymers 15 (6) (2023) 1549, https://doi.org/10.3390/polym15061549.
[47] K.V. Vydehi, A.A.B. Moghal, B.M. Basha, Target reliability-based design of embankments using biopolymer-modified cohesive soil, Int J. Geomech. 22 (8) (2022) 04022115, https://doi.org/10.1061/(ASCE)GM.1943-5622.0002429.
[48] J. Del Viso, J. Carmona, G. Ruiz, Shape and size effects on the compressive strength of high-strength concrete, Cem. Concr. Res 38 (3) (2008) 386–395, https://doi.org/10.1016/j.cemconres.2007.09.020.
[49] ASTM, Standard Test Method for Unconfined Compressive Strength of Cohesive Soil, ASTM International, West Conshohocken, PA, 2016.
[50] B. Indraratna, R. Athukorala, J. Vinod, Estimating the rate of erosion of a silty sand treated with lignosulfonate, J. Geotech. Geoenviron. Eng. 139 (5) (2013) 701–714, https://doi.org/10.1061/(ASCE)GT.1943-5606.0000766.
[51] R. Gedela, B. Indraratna, S. Medawela, T.T. Nguyen, Effects of fines content on the strength and stiffness of biopolymer treated low-plasticity soils, Aust. Geomech. J. 58(1 (2023) 33–41, https://doi.org/10.56295/Agj5811.
[52] A.M. Donald, The use of environmental scanning electron microscopy for imaging wet and insulating materials, Nat. Mater. 2 (8) (2003) 511–516, https://doi.org/10.1038/nmat898.
[53] ASTM, Standard Practice for Describing and Measuring Performance of Fourier Transform Mid-infrared (FT-MIR) Spectrometers Level Zero and Level One Tests, ASTM International, West Conshohocken, PA, 2021.
[54] T. Chompoorat, T. Thepumong, S. Taesinlapachai, S. Likitlersuang, Repurposing of stabilised dredged lakebed sediment in road base construction, J. Soils Sediment. 21 (7) (2021) 2719–2730, https://doi.org/10.1007/s11368-021-02974-3.
[55] G.C. Cho, J.C. Santamarina, Unsaturated particulate materials - particle-level studies, J. Geotech. Geoenviron. Eng. 127 (1) (2001) 84–96, https://doi.org/10.1061/(ASCE)1090-0241(2001)127:1(84).
[56] I. Chang, J. Im, G.-C. Cho, Geotechnical engineering behaviors of gellan gum biopolymer treated sand, Can. Geotech. J. 53 (10) (2016) 1658–1670, https://doi.org/10.1139/cgj-2015-0475.
[57] J.R. Gales, T.S. Young, G.P. Willhite, D.W. Green, Equilibrium swelling and syneresis properties of Xanthan gum/Cr(III) gels, SPE Adv. Technol. Ser. 2 (02) (1994) 190–198, https://doi.org/10.2118/17328-pa.
[58] F. Garver, M. Sharma, G. Pope, The competition for chromium between xanthan biopolymer and resident clays in sandstones, in: Proceedings of the SPE Annual Technical Conference and Exhibition, SPE, 1989, SPE-19632-MS, https://doi.org/10.2118/SPE-19632-MS.
[59] W.F. Pu, Y. Yang, C.D. Yuan, Gelation performance of poly (ethylene imine) crosslinking polymer–layered silicate nanocomposite gel system for potential water-shutoff use in high-temperature reservoirs, J. Appl. Polym. Sci. 133 (47) (2016), https://doi.org/10.1002/app.44243.
[60] K. Kabiri, H. Mirzadeh, M.J. Zohuriaan-Mehr, M. Daliri, Chitosan-modified nanoclay–poly (AMPS) nanocomposite hydrogels with improved gel strength, Polym. Int. 58 (11) (2009) 1252–1259, https://doi.org/10.1002/pi.2652.
[61] C.S. Chang, J.Y. Wang, L. Ge, Modeling of minimum void ratio for sand-silt mixtures, Eng. Geol. 196 (2015) 293–304, https://doi.org/10.1016/j.enggeo.2015.07.015.
[62] I. Chang, G.-C. Cho, Shear strength behavior and parameters of microbial gellan gum-treated soils: from sand to clay, Acta Geotech 14 (2) (2019) 361–375, https://doi.org/10.1007/s11440-018-0641-x.
[63] D. Kim, B.H. Nam, H. Youn, Effect of clay content on the shear strength of clay–sand mixture, Int. J. Geo Eng. 9 (1) (2018) 19, https://doi.org/10.1186/s40703-018-0087-x.
[64] A. Soldo, M. Miletic, Durability against wetting-drying cycles of sustainable biopolymer-treated soil, Polymers 14 (19) (2022) 4247, https://doi.org/10.3390/polym14194247.
[65] Y.-M. Kwon, I. Chang, G.-C. Cho, Consolidation and swelling behavior of kaolinite clay containing xanthan gum biopolymer, Acta Geotech. (2023), https://doi.org/10.1007/s11440-023-01794-8.
[66] T. Pongjanyakul, S. Puttipipatkhachorn, Xanthan-alginate composite gel beads: molecular interaction and in vitro characterization, Int J. Pharm. 331 (1) (2007) 61–71, https://doi.org/10.1016/j.ijpharm.2006.09.011.
[67] H.H. Darzi, S.G. Larimi, G.N. Darzi, Synthesis, characterization and physical properties of a novel xanthan gum/polypyrrole nanocomposite, Synth. Met. 162 (1-2) (2012) 236–239, https://doi.org/10.1016/j.synthmet.2011.12.004.
[68] A. Kumar, M. Ahuja, Carboxymethyl gum kondagogu: Synthesis, characterization and evaluation as mucoadhesive polymer, Carbohydr. Polym. 90 (1) (2012) 637–643, https://doi.org/10.1016/j.carbpol.2012.05.089.
[69] M. Kang, O. Oderinde, S. Liu, Q. Huang, W. Ma, F. Yao, G. Fu, Characterization of xanthan gum-based hydrogel with Fe^{3+} ions coordination and its reversible sol-gel conversion, Carbohydr. Polym. 203 (2019) 139–147, https://doi.org/10.1016/j.carbpol.2018.09.044.
[70] D. Kim, M. Sagong, Y. Lee, Effects of fine aggregate content on the mechanical properties of the compacted decomposed granitic soils, Constr. Build. Mater. 19 (3) (2005) 189–196, https://doi.org/10.1016/j.conbuildmat.2004.06.002.
[71] J. Gregory, S. Barany, Adsorption and flocculation by polymers and polymer mixtures, Adv. Colloid Interface Sci. 169 (1) (2011) 1–12, https://doi.org/10.1016/j.cis.2011.06.004.
[72] X.X. He, J.F. Xue, M.J. Liao, Y. Wan, X.L. Liu, Y.J. Chen, Q. Xue, Strength and hygroscopic behavior of biopolymer-treated silty sand under remodeling and dry-wet cycles, Constr. Build. Mater. 408 (2023) 133642, https://doi.org/10.1016/j.conbuildmat.2023.133642.
[73] J. Kristó, R.L. Frost, A. Felinger, J. Mink, FTIR spectroscopic study of intercalated kaolinite, J. Mol. Struct. 410 (1997) 119–122, https://doi.org/10.1016/S0022-2860(96)09488-4.
[74] J.M. Duncan, C.-Y. Chang, Nonlinear analysis of stress and strain in soils, J. Soil Mech. Found. Div. 96 (5) (1970) 1629–1653, https://doi.org/10.1061/JSFEAQ.0001458.
[75] B. Yoon, W. Lee, C. Lee, H. Choo, Time-dependent variations of compressive strength and small-strain stiffness of sands grouted with microfine cement, J. Geotech. Geoenviron. Eng. 146 (4) (2020), https://doi.org/10.1061/(ASCE)GT.1943-5606.0002207.
[76] M. Marudova-Zsivanovits, N. Jilov, E. Gencheva, Rheological investigation of xanthan gum–chromium gelation and its relation to enhanced oil recovery, J. Appl. Polym. Sci. 103 (1) (2007) 160–166, https://doi.org/10.1002/app.25025.
[77] A. Neramitkornburi, S. Horpibulsuk, S.L. Shen, A. Chinkulkijniwat, A. Arulrajah, M.M. Disfani, Durability against wetting-drying cycles of sustainable lightweight cellular cemented construction material comprising clay and fly ash wastes, Constr. Build. Mater. 77 (2015) 41–49, https://doi.org/10.1016/j.conbuildmat.2014.12.025.
[78] P. Bagheri, I. Gratchev, S. Son, M. Rybachuk, Durability, strength, and erosion resistance assessment of lignin biopolymer treated soil, Polymers 15 (6) (2023) 1556, https://doi.org/10.3390/polym15061556.
[79] S. Lee, I. Chang, M.-K. Chung, Y. Kim, J. Kee, Geotechnical shear behavior of Xanthan Gum biopolymer treated sand from direct shear testing, Geomech. Eng. 12 (5) (2017) 831–847, https://doi.org/10.12989/gae.2017.12.5.831.
[80] S. Seo, M. Lee, J. Im, Y.-M. Kwon, M.-K. Chung, G.-C. Cho, I. Chang, Site application of biopolymer-based soil treatment (BPST) for slope surface protection: in-situ wet-spraying method and strengthening effect verification, Constr. Build. Mater. 307 (2021), https://doi.org/10.1016/j.conbuildmat.2021.124983.
[81] M. Lee, I. Chang, S.-J. Kang, D.-H. Lee, G.-C. Cho, Alkaline induced-cation crosslinking biopolymer soil treatment and field implementation for slope surface protection, Geomech. Eng. 33 (1) (2023) 29–40, https://doi.org/10.12989/gae.2023.33.1.029.
[82] J. Ni, G.-L. Hao, J.-Q. Chen, L. Ma, X.-Y. Geng, The optimisation analysis of sand-clay mixtures stabilised with xanthan gum biopolymers, Sustainability 13 (7) (2021) 3732, https://doi.org/10.3390/su13073732.
[83] J. Ni, S.-S. Li, X.-Y. Geng, Mechanical and biodeterioration behaviours of a clayey soil strengthened with combined carrageenan and casein, Acta Geotech. 17 (12) (2022) 5411–5427, https://doi.org/10.1007/s11440-022-01588-4.